HHS Public Access

Author manuscript

Free Radic Biol Med. Author manuscript; available in PMC 2015 April 20.

Published in final edited form as:

Free Radic Biol Med. 2014 March ; 68: 302–314. doi:10.1016/j.freeradbiomed.2013.11.031.

Mn Porphyrin in combination with ascorbate acts as a pro-oxidant and mediates caspase-independent cancer cell death

Myron K. Evans[1,2], **Artak Tovmasyan**[3], **Ines Batinic-Haberle**[3,4,§], and **Gayathri R. Devi**[1,2,4,§]

[1]Department of Surgery, Duke University Medical Center, Durham, NC 27710, USA

[2]Department of Pathology, Duke University Medical Center, Durham, NC 27710, USA

[3]Department of Radiation Oncology, Duke University Medical Center, Durham, NC 27710, USA

[4]Duke Cancer Institute, Duke University Medical Center, Durham, NC 27710, USA

Abstract

Resistance to therapy-mediated apoptosis in inflammatory breast cancer (IBC), an aggressive and distinct subtype of breast cancer, was recently attributed to increased superoxide dismutase (SOD) expression, glutathione (GSH), and decreased accumulation of reactive species. In the present study, we demonstrate the unique ability of two Mn(III) *N*-substituted pyridylporphyrin (MnP)-based SOD mimics (MnTE-2-PyP^{5+} and MnTnBuOE-2-PyP^{5+}) to catalyze oxidation of ascorbate, leading to the production of excessive levels of peroxide and in turn cell death. The accumulation of peroxide, as a consequence of MnP + ascorbate treatment, was fully reversed by the administration of exogenous catalase showing that ROS was essential for cell death. Cell death as a consequence of the action of MnP/ascorbate corresponded with decreases in GSH levels, pro-survival signaling (pNF-κB, pERK1/2), and in expression of X-linked inhibitor of apoptosis protein (XIAP), the most potent caspase inhibitor. Although markers of classical apoptosis were observed, including PARP cleavage and Annexin V staining, administration of a pan-caspase inhibitor, QVD-OPh, did not reverse the observed cytotoxicity. MnP + ascorbate treated cells showed nuclear translocation of apoptosis inducing factor (AIF), suggesting the possibility of a mechanism of caspase-independent cell death. Pharmacological ascorbate has already shown promise in recently completed Phase I Clinical Trials, where its oxidation and subsequent peroxide formation was catalyzed by endogenous metalloproteins. The catalysis of ascorbate oxidation by an optimized metal-based catalyst (such as Mn porphyrin) carries a large therapeutic potential as a sole anticancer agent or in combination with other modalities such as radio- and chemo- therapy.

[§]Corresponding authors: Address manuscript correspondence to Gayathri R. Devi, Department of Surgery, Division of Surgical Sciences, 2606 DUMC Duke University Medical Center, Durham, NC, 27710. gayathri.devi@duke.edu or Ines Batinic-Haberle, Department of Radiation Oncology, 3455 DUMC Duke University Medical Center, Durham, NC, 27710. ibatinic@duke.edu.

Conflict of interest

Dr. Batinic-Haberle is a consultant for BioMimetix Pharmaceutical, Inc., and, along with Duke University, has patent rights of this technology licensed to BioMimetix.

Keywords

manganese porphyrins; ascorbate; apoptosis; SUM149; SUM190; inflammatory breast cancer; XIAP; ROS; SOD

INTRODUCTION

At physiological low levels, reactive species function as “redox messengers” in intracellular signaling and homeostatic regulation. In contrast, when cells are exposed to or accumulate high levels of ROS in submicro- and micro- molar concentrations, the oxidative modification of cellular macromolecules, inhibition of protein function, and cell death can occur [1-4]. Therefore, increased accumulation of ROS leading to cancer cell death is a prominent mechanism of radiotherapy and many commonly used chemotherapeutics [5-8]. Cells, however, have an innate ability to regulate ROS and modulate apoptosis using various redox systems which operate on multiple levels, including but not limited to glutathione (GSH), glutathione peroxidases (GPx), thioredoxins (Trx), peroxiredoxins (Prx), catalases and superoxide dismutases (SODs); this redox balance is frequently deregulated in cancer cells, leading to the therapeutic resistance [9, 10]. It is observed that in cancer cells, a robust redox adaptation often evolves as a survival mechanism which leads to an upregulation of antioxidant capacity and a shift of redox dynamics (low ROS generation combined with higher rate of elimination). This allows for maintenance of ROS levels below the threshold needed to induce cell death [11, 12].

We recently reported this mechanism to be highly prevalent in a model of aggressive breast cancer called inflammatory breast cancer (IBC), wherein therapeutic resistance was identified to result from increased antioxidants (such as GSH, SOD1 and SOD2) coupled with insignificant ROS accumulation [13]. Since cancer cells are more dependent on antioxidant systems than other non-transformed cells, and are especially vulnerable to increased oxidative stress, development of exogenous ROS modulatory systems that can elevate intratumoral ROS levels above the threshold associated with therapeutic apoptosis is an attractive therapeutic strategy to selectively kill cancer cells [12, 14-17]

SOD is the first line of cellular anti-oxidative defenses and thus controls not only levels of $O_2^{\bullet-}$ but also its progeny [18]. Therefore, small molecules mimicking its function have been developed over the last 2 decades in order to augment cellular antioxidant capacity. Cationic Mn(III) *N*-substituted pyridyl- and *N,N’*-disubstituted imidazolyl- porphyrins are among the most potent synthetic SOD mimics identified to date [14, 19-21]. They target both cytoplasmic and mitochondrial compartments, where they can catalyze the dismutation of $O_2^{\bullet-}$ at similar efficacy to the endogenous SOD proteins. During $O_2^{\bullet-}$ dismutation, a potent SOD mimic reduces and oxidizes $O_2^{\bullet-}$ with similar reaction constants to the endogenous enzyme [22]. As $O_2^{\bullet-}$ is only a mild anti- and pro-oxidant, such reactivity makes SOD mimics mild anti- and pro- oxidants; this in fact suggests that a powerful SOD mimic would be a perfect modulator of the cellular redox environment, modulating electron trafficking within the cell [19]. *In vivo*, due to the high levels of cellular reductants, such as thiols and ascorbate, SOD mimics will be reduced to $Mn^{II}P$ with ascorbate and thiols in a 1^{st} step

(rather than with $O_2^{\bullet-}$), and re-oxidized to $Mn^{III}P$ with $O_2^{\bullet-}$ in a 2nd step of dismutation process, giving rise to H_2O_2. Due to the high *in vivo* concentration of oxygen, $Mn^{II}P$ may also be preferably re-oxidized in a 2nd step with oxygen giving rise to $O_2^{\bullet-}$ and subsequently to H_2O_2 again. If the cell is not able to remove this peroxide, a state of oxidative stress will occur. In other instances, cells may benefit from MnP-based SOD mimic in a similar fashion as from endogenous SOD enzymes. The comparison of MnP-based SOD mimics to natural SOD enzymes is valid because they possess nearly identical thermodynamics and similar electrostatics for $O_2^{\bullet-}$ dismutation [23]. It has indeed been shown that in many cancer cells, which frequently have peroxide-removing enzymes downregulated (as opposed to normal cells), the overexpression of MnSOD results in increased H_2O_2 production [14, 15].

When MnPs are administered in combination with exogenous ascorbate, as in our experiments, they may no longer function as a mimic of an “antioxidant” SOD enzyme. The production of peroxide may be overwhelming for the cell and the cell would likely undergo death; such pro-oxidative effects of MnP/ascorbate have previously been explored for anticancer therapy [24-27]. Indeed, ascorbate was used as an anticancer drug in Phase I Clinical trials that have been recently completed. Here, the oxidation of ascorbate, which results in peroxide formation, was catalyzed by endogenous metalloproteins [23, 28, 29].

Herein, we explore two different Mn porphyrins in combination with ascorbate with the following goals: (1) to optimize peroxide production and in turn induce cell death in an aggressive subtype of breast cancer (inflammatory breast cancer); and (2) to explore the cellular pathways involved in cell death. In addition to the degree of optimization of MnP/asc system, the magnitude of the cell death may depend upon the redox status of the cell (balance between ROS and endogenous anti-oxidative defenses), the species MnP would encounter, and the localization of MnP within the cell. Our results reveal that ROS accumulation is a consequence of MnP and ascorbate treatment, as cytotoxicity was fully reversed in the presence of exogenous catalase. We also elucidate the molecular mechanisms that drive the cytotoxicity of this combination in aggressive breast cancer cells and therapy-resistance cells, including but not limited to the downregulation of NF-κB and ERK signaling, showing that the excessive peroxide production can overcome mechanisms of acquired therapeutic resistance in IBC.

MATERIALS AND METHODS

Cell lines

SUM149 and SUM190 cells were obtained from Asterand, Inc. (Detroit, MI) and were cultured as previously described [30]. Characterization and authentication of the cell lines were done at Asterand by short tandem repeat polymorphism analysis. Cells were banked upon receipt and cultured for no more than 6 months prior to use in this study. rSUM149 is an isogenic model derived from SUM149 in the lab and cultured as previously described [31]. All cells were cultured at 37 °C, 5% CO_2.

MnP-based SOD mimics

Two Mn porphyrins, MnTE-2-PyP^{5+} (AEOL10113, BMX-010) and MnTnBuOE-2-PyP^{5+} (BMX-001), have been synthesized, purified and characterized by means of thin-layer chromatography, elemental analysis, ESI-MS, and UV-Vis spectroscopy as earlier described [32, 33]. The structures and properties of both Mn porphyrins are presented in Figure 1: catalytic rate constant for $O_2^{\bullet-}$ dismutation, $k_{cat}(O_2^{\bullet-})$; rate constant for the reduction of O_2 to $O_2^{\bullet-}$, $k_{red}(O_2)$; metal-centered reduction potential for $Mn^{III}P/Mn^{II}P$, $E_{1/2}$ in mV *vs.* NHE; and lipophilicity as characterized by partition coefficient for n-octanol and water, log P_{ow}.

Treatment of cells for determination of viability, proliferation, and signaling analysis

Cells were seeded in either 6-well or 12-well plates (Corning Incorporated, Corning, NY) and allowed to reach ~80% confluence. Cells were then treated for 4 h or 24 h, as indicated, in growth media with MnPs (either MnTE-2-PyP^{5+} or MnTnBuOE-2-PyP^{5+}) or sodium L-ascorbate (Sigma, St. Louis, MO, abbreviation *ascorbate* or *asc* was used throughout text as well as chemical formula HA^- which represents the major species under physiological pH conditions) alone and in combination. The stock solution of ascorbate was made fresh prior to each experiment. The concentrations of MnPs and ascorbate explored in this study was based on our earlier studies [24]. Pan-caspase inhibitor Q-VD-OPh (Calbiochem, San Diego, CA) was added to cells 30 minutes prior to treatment with staurosporine or MnP+asc combination. Catalase (Sigma) was added 15 minutes prior to treatment with MnP+asc combination. Trypan blue exclusion assay was used to determine cell viability as described previously [30]. MTT assay was used to determine cellular proliferation, metabolic activity, and reduction capacity as described previously [30, 34].

Western immunoblot analysis

Immunoblot analysis was carried as described previously [31]. Cell lysates were harvested after the indicated treatments for 4 h. Membranes were incubated with primary antibodies against NF-κB, *p*-NF-κB, p44/42 (ERK1/2), *p*-p44/42 (*p*-ERK1/2), p38 (MAPK), *p*-p38 (*p*-MAPK), PARP, SOD1 (Cell Signaling Technologies, Danvers, MA, 1:1000), SOD2, XIAP (BD Bioscience, San Jose, CA, 1:1000 and 1:2000, respectively), or GAPDH (Santa Cruz Biotechnology Inc., Santa Cruz, CA, 1:4000), overnight at 4 °C. Membranes were washed and incubated with anti-mouse or anti-rabbit HRP-conjugated antibodies (Cell Signaling Technologies) for 1 h at room temperature. Chemiluminescent substrate (Thermo Scientific, Waltham, MA) was applied for 5 minutes, and membranes were exposed to film. Stripping of membranes for detection of total protein was done as previously described [34]. Densitometric analysis was performed using the NIH ImageJ software [35].

Glutathione content assay

GSH levels were assessed as described previously [13, 36], after 4 h treatment of the cells, using the GSH-Glo Assay (Promega, Madison, WI) as per the manufacturer's instructions. Equal amount of protein lysate (3 μg) was loaded for each treatment.

Spectrophotometrical study of the reaction of MnPs with ascorbate

The time-dependent spectral change of MnP/ascorbate system for both E2 and BuOE2 was followed. The time-dependent content of MnP (%) catalyst was determined based on the disappearance of the absorbance of reduced E2 at 438 nm and BuOE2 at 441.5 nm as previously reported [24, 37, 38]. The oxidation/consumption of ascorbate (%) was followed spectrally at 265 nm. Also the initial rates for ascorbate oxidation were determined at 265 nm. The reduction and eventual destruction of MnPs (6 μM) was followed in the presence of ascorbate (0.42 mM) at pH 7.8 (maintained by 0.05 M Tris buffer) on a UV-2550 PC spectrophotometer (0.5 nm resolution) (Shimadzu Instruments, Columbia, MD). While high concentrations of MnP could not have been used in aqueous system, as too high absorbance above 4 could not be measured, the ratio of MnP to ascorbate was kept the same in aqueous and cellular systems.

Detection of Phosphatidylserine Exposure

Cells were cultured in 6-well plates and allowed to reach ~80% confluence. Cells were treated with the indicated agents for 4 h, then harvested and incubated for five minutes with Annexin V-biotin staining solution (Immunotech, Marseilles, France**)**. Cells were washed with 1% BSA/PBS and then incubated 15 min on ice with streptavidin-FITC (Zymed, San Francisco, CA). Cells were washed and analyzed by flow cytometry. Again, at least 25,000 events were collected; the total cell population was used for analysis.

Apoptosis Inducing Factor (AIF) Immunofluorescence

Cells were plated on coverslips (VWR, Radnor, PA) that had previously been coated with Poly-L-Lysine (Sigma) and stored in 70% ethanol. The next day, treatments were added for 4 h, and cells were fixed using 4% formaldehyde for 20 minutes. Blocking and permeabilization was performed with a solution of PBS containing 0.1% Triton X-100 and 5% normal goat serum. Anti-AIF antibody (Cell Signaling Technologies, 1:400), diluted in blocking buffer, was added to the cells overnight. After two washes with PBS, anti-mouse FITC secondary (Jackson Immunoresearch, West Grove, PA, 1:200, kindly provided by Dr. Jack Keene, Duke) was added for 1h. The coverslips were washed with PBS, mounted on slides with Prolong® Gold Antifade with DAPI (Invitrogen, Grand Island, NY), and imaged with a Zeiss AxioObserver (Zeiss, Thornwood, NY) complete with imaging software analysis package. H_2O_2 (500μM) was used as positive control.

Statistical Analysis

All statistical analyses were performed using GraphPad Prism software (Graphpad, La Jolla, CA). Differences were considered significant at $p<0.05$.

RESULTS

Combination of SOD mimic+asc decreases cell viability of therapy -sensitive and -resistant IBC cells

We evaluated both MnTE-2-PyP^{5+} (E2) and MnTnBuOE-2-PyP^{5+} (BuOE2) (whose distinct physical and chemical characteristics are shown in Figure 1) in cellular models of IBC, a

highly aggressive breast cancer subtype with increased deregulation in apoptotic and oxidative response gene signaling [13, 30, 39, 40]. The cell lines tested are SUM190 (ErbB2 overexpressing), SUM149 (basal type), which are well established IBC models isolated from patient primary tumors and rSUM149, an isogenic derivative that shows significant resistance to ROS-mediated apoptosis due to high levels of key antioxidants (GSH, SOD1, SOD2) when compared to parental SUM149 cells [13, 31, 40]. We first characterized cell viability with increasing doses (0-50 μM) of the two MnPs in combination with ascorbate by trypan blue exclusion assay (Figure 2). Neither of the MnPs or ascorbate alone had a significant effect on viability in any of the cell lines (data not shown). Data in Figure 2 (A-C) show that both E2 and BuOE2 in combination with ascorbate caused decreased viability in all three cell lines. The E2 compound, however, decreased viability at lower concentrations (EC_{50} of 10 μM for E2 as compared to 30 μM of BuOE2). The viability data in Figure 2 (A-C) agrees well with the ~4-fold higher $k_{red}(O_2)$ for E2 (Figure 1). Table 1 lists the approximate, calculated EC_{50} values for each combination across the cell lines.

In three cell lines tested, ascorbate alone increased formation of formazan (the purple colored reduced tetrazolium MTT reagent measured as explained in Methods section) (~30-50% over untreated) which is commonly used to measure the cellular reducing potential as well as proliferation (Figure 2, D-F) [41]. E2 alone also increased the reduction of MTT dye to formazan in both SUM149 and SUM190 cell lines (~40% over untreated), but not in the therapy-resistant rSUM149 line, while BuOE2 alone caused no significant increase in any of the three cell lines. When combined with ascorbate, E2 induced a significant decrease when compared to E2 alone (~ 70-120% decrease), while BuOE2 yielded a lower decrease (~30-45%). We also assessed increased proliferation by total cell counts and observed results are similar to those shown in Figure 2D-F. The administration of MnPs decreased the growth rate for cells ~4 hours, bringing the SUM149 line doubling time from 22.5 hours to 17.5 hours (data not shown). The cytotoxic pro-oxidative effects were not seen with either of the MnPs as single agents at given concentrations.

H_2O_2 is essential for MnP+asc cytotoxicity and decreases pro-survival signaling in IBC cells

As it has been previously postulated that the combination of MnP and ascorbate acts as a pro-oxidant, we tested the levels of endogenous antioxidant defenses in the cells after treatment with E2+asc. Western immunoblot of SOD1 and SOD2 show that in SUM149 cells, addition of excess ascorbate, either alone or in combination with MnPs actually caused increased SOD1 expression (Figure 3A, *top*). E2 alone also produced a slight increase in SOD1 expression. This slight upregulation is most likely a response to ROS accumulation in the cell. SOD2 expression showed no significant changes under any of the indicated conditions (Figure 3A, *middle*). We also assessed levels of glutathione (GSH) in the cells after treatment. Neither ascorbate nor E2 alone had any effect on GSH levels, however, the combination of E2+asc significantly depleted GSH levels in the SUM149 cells, which correlates with oxidant accumulation (Figure 3B).

In order to prove H_2O_2 involvement in MnP+asc cytotoxicity, we examined whether the administration of exogenous catalase, an H_2O_2 scavenger, would reverse the cell death. Data

in Figure 3C show that the treatment of cells with E2+asc and BuOE2+asc in the presence of catalase provided protection against the H_2O_2-mediated cell death and significantly increased the cellular viability ($p<.01$ and $p<.05$, respectively) (Figure 3C).

Since the E2+asc combination leads to excessive H_2O_2 production and in turn decreased cell viability, western immunoblot was carried out to elucidate the expression of proteins involved in ROS and cell survival signaling. Immunoblots in Figures 4A, B, and C show a dose-dependent decrease in ERK1/2 phosphorylation [p44/42]), nuclear factor kappa-light-chain-enhancer of activated B cells phosphorylation (NF-κB), but no significant changes in p38 MAPK phosphorylation in E2+asc treated lysates, respectively, which is consistent with the increased ROS production and decreased viability.

MnP+asc-induced apoptosis is caspase independent and correlates with AIF translocation

As the E2+asc combination exhibited high cytotoxicity in the aggressive breast cancer cells tested, Annexin V staining (marker of early apoptosis) was carried out with E2, alone and in combination with ascorbate to gain further insight into the mechanism of cell death. Figure 5A shows a dose-dependent increase in the number of Annexin V positive cells in the SUM149 cells. Analysis of X-linked inhibitor of apoptosis (XIAP) expression, the most potent cellular inhibitor of apoptosis, in SUM149 cells showed a decrease in XIAP expression with the combination of E2+asc (Figure 5B top panel). BuOE2+asc, however, had little to no effect (data not shown). A cleavage product of XIAP was also observed in E2+asc treated cells at both doses, while BuOE2+asc showed negligible cleavage. PARP cleavage is another marker of apoptosis that was measured to elucidate the mechanism of cell death. Combination of E2 and ascorbate at lower doses led to a decrease in total PARP expression and as the concentration of the combination increased to a dose corresponding to the EC_{50}, PARP cleavage as well as a laddering effect was observed (Figure 5B, middle panel).

Interestingly, MnP+asc mediated cell death was not reversed when cells were pre-treated with a pan-caspase inhibitor (QVD-OPh). Staurosporine, a known apoptosis inducer that is semi-dependent on the caspase activity [42], was used as a control, and pre-treatment with QVD-OPh significantly reversed staurosporine-mediated cell death, while having no significant effects on cell death mediated by MnP+asc combination (Figure 5C).

Given that caspase inhibition did not reverse the cell death seen with combination treatment, we sought to investigate the possibility of a caspase-independent mechanism of apoptosis. To further characterize the cell death mechanism, cells were treated and immunostained for apoptosis inducing factor (AIF) following treatment with MnP+asc. Translocation to the nucleus was indicated by the overlap of the AIF fluorescent signal (FITC) with DAPI nuclear staining. H_2O_2 was used as a positive control, as it has been previously linked to caspase-independent cell death and AIF translocation [43, 44]. In untreated cells (Figure 6 top panel), AIF was seen to surround the nucleus in a pattern consistent with the normal mitochondrial localization of the protein. However, upon treatment with H_2O_2 or MnP+asc, AIF translocated into the nucleus, and staining overlapped with DAPI (Figure 6, middle and lower panels).

Ascorbate oxidation/consumption catalyzed by E2 is moderately faster than by BuOE2

In order to further understand the differences in cytotoxicity and ROS production between E2 and BuOE2, we spectrophotometrically measured the loss of MnP at 438 nm for E2 and 441.5 nm for BuOE2, which correspond to Soret bands of reduced Mn^{II}Ps (Figure 7A). The data in Figure 7A only relate to the presence of reduced Mn^{II}P in solution, but did not account for species which bear Mn in +3, +4, and +5 oxidation states. With ascorbate in solution only reduced Mn^{II}P was detected (Figure 7B). Once ascorbate is fully consumed (detected as disappearance of HA^- absorption band at 265 nm), we saw the appearance of Mn^{III}P at 90 min for E2 and 125 min for BuOE2 (Figure 7B). The H_2O_2, which is produced as a consequence of MnP/ascorbate cycling, oxidizes Mn^{III}P to $(O)_2Mn^{V}$P [49,50,51]. Mn in $(O)_2Mn^{V}$P then oxidizes the porphyrin ring which in turn falls apart [45]. Aside from Mn^{II}P and Mn^{III}P, which were clearly detected spectrally, other features of a complicated spectrum relate to the high-valent Mn oxo species (Figure 7B). We also assessed the oxidation/consumption of ascorbate (HA^-) spectrally as the disappearance of its absorption band at 265 nm (Figure 7C) *via* initial rates approach. The initial rates, $v_o(HA^-)_{ox}$ are given in Figure 1B. The differences in initial rates of ~30% between E2 ($v_o(HA^-)_{ox} = 1.7 \times 10^{-7}$ M s^{-1}) and BuOE2 ($v_o(HA^-)_{ox} = 1.2 \times 10^{-7}$ M s^{-1}) (Figure 7B). The $E_{1/2}$ of BuOE2, relative to E2, is ~50 mV more positive; this indicates that it is more electron-deficient than E2 and likes accepting electron. Therefore, the BuOE2 is stabilized in the Mn +2 oxidation state more than E2. In turn, it would be less prone to re-oxidation with O_2 (eq [3]) and peroxide formation than E2, thus to peroxide-driven oxidative degradation. Based on the estimated rate constant for Mn^{II}P re-oxidation with O_2 to Mn^{III}P [eq [3]), $k_{red}(O_2)$ (Figure 1B) [46], presumably the rate-limiting step in peroxide production, the ~2.6-fold faster H_2O_2 production by E2 than by BuOE2 may be anticipated. The estimation of $k_{red}(O_2)$ is based on the Marcus equation and suffers from the limitations (See Discussion under subtitle E2 vs. BuOE2). Yet, the data on the metabolic activity (MTT assay, Figure 2) and cell viability (trypan blue exclusion assay, Figure 2 and 3) agree well with such estimation; they indicate that: (i) 10 μM E2+asc inflicts equal loss of cell viability as 30 μM BuOE2+asc (Figure 3); and (ii) 30 μM BuOE2+asc is up to few-fold less cytotoxic than 30 μM E2+asc (Figure 2).

The ascorbate oxidation, H_2O_2 production and subsequent MnP degradation

The favorable properties of the catalyst would involve not only the rate of ascorbate oxidation and in turn H_2O_2 production, but also the rate of its oxidative degradation. As long as it is present in solution, ascorbate supports Mn^{III}P/Mn^{II}P and suppresses Mn^{III}P/$(O)_2Mn^{V}$P redox (Figures 7A and B). Once ascorbate is oxidized/consumed (at ~90 or 125 min, respectively for E2 and BuOE2) (Figure 7C), the Mn^{III}P starts undergoing oxidation to $(O)_2Mn^{V}$P with subsequent porphyrin ring degradation (Figures 7A and B) [45]. The $(O)_2Mn^{V}$P was identified as two-electron oxidized species based on the H_2O_2/MnP kinetic studies of a very similar MnTDE-2-ImP^{5+} analog [23, 47]. The $(O)_2Mn^{V}$P readily decays to O=Mn^{IV}P [48, 49]. *In vitro* and *in vivo* the high-valent Mn oxo species cycles back to Mn^{III}P with cellular reductants [49]. Once ascorbate is consumed, thus H_2O_2 accumulated, the spectral scans show similar spectral profiles to those obtained in MnP+ H_2O_2 system. The MnP degradation in the presence of MnP/asc and MnP/H_2O_2 shows the same spectrophotometrical profile [32, 37, 38], which is additional proof that peroxide is produced

in the reaction of MnP with ascorbate [24, 37, 50]. The BuOE2 is less prone to re-oxidation from $Mn^{II}P$ to $Mn^{III}P$ than E2. Therefore, within same time period its catalytic action upon ascorbate oxidation results in lower peroxide levels than with E2. Thus, oxidative degradation of BuOE2 begins with certain delay (~30 min), which gives impression that it appears more resistant in the reaction mixture than E2. More studies are needed to gain further insight into its resistance towards oxidative degradation with H_2O_2 relative to other Mn(III) *N*-substituted pyridylporphyrins..

DISCUSSION

We report herein the assessment of the cytotoxic effects of two MnPs in combination with ascorbate on inflammatory breast cancer cells and the pathways involved in cell death mediated by this combination. Two MnPs of different physical and chemical properties listed in Figure 1 were explored in order to understand their ability to act as catalysts for ascorbate oxidation and peroxide formation. We have previously reported the reducibility of cationic Mn(III) *N*-substituted pyridylporphyrins with cellular reductants and our data suggest that the MnP+asc system may represent a prospective anticancer treatment for aggressive inflammatory breast cancer [22, 23, 32, 51].

Switch from the SOD-like “anti-oxidative” effects of MnP to cell-killing pro-oxidative effects

During $O_2^{\bullet-}$ dismutation, a powerful SOD mimic (such as MnTE-2-PyP^{5+} or MnTnBuOE-2-PyP^{5+}) (Figure 1) with $E_{1/2}$ at ~midway potential between the oxidation and reduction of $O_2^{\bullet-}$ (~ 300 mV *vs*. NHE) (Figure 1B) [22] favors reducing and oxidizing superoxide to a similar extent, thus acting as both a mild pro- and anti-oxidant (Figure 8A and B). Due to the high mM levels of intracellular reductants, MnPs would prefer coupling with them and acting as superoxide reductase, rather than superoxide dismutase, eqs [1] and [2]. Thus, instead of oxidizing $O_2^{\bullet-}$, MnP would oxidize ascorbate (HA^-) in a 1st step of dismutation process [eq 1], and will reduce $O_2^{\bullet-}$ in a 2nd step (eq [2]) [14, 19, 20, 23]:

$$Mn^{III}\mathrm{P}^{5+}+HA^- \iff Mn^{II}\mathrm{P}^{4+}+HA^{\bullet}, \quad v_o(HA^-)_{ox} \quad [1]$$

$$HA^{\bullet} \iff \mathrm{A}^{\bullet-}+\mathrm{H}^+, \quad pK_a(HA^{\bullet}) = -0.45 \quad [1a]$$

$$Mn^{III}\mathrm{p}^{5+}+\mathrm{A}^{\bullet-} \iff Mn^{II}\mathrm{p}^{4+}+\mathrm{A} \quad [1b]$$

$$Mn^{II}\mathrm{P}^{4+}+2\ \mathrm{H}^+ + \mathrm{O_2}^{\bullet-} \iff Mn^{III}\mathrm{P}^{5+}+\mathrm{H_2O_2}, \quad \text{superoxide reductase activity of MnP} \quad [2]$$

$$Mn^{II}\mathrm{P}^{4+}+\mathrm{O_2} \iff Mn^{III}\mathrm{P}^{5+}+\mathrm{O_2}^{\bullet-}, \quad k_{red}(\mathrm{O_2}) \quad [3]$$

$$\mathrm{A}^{\bullet-}+\mathrm{O_2} \iff \mathrm{A}+\mathrm{O_2}^{\bullet-}; \quad [4]$$

$$2\ \ O_2^{\bullet -} + 2\ \ H^+ \iff O_2 + H_2O_2 \quad [4a]$$

In a 2nd step, under aerobic conditions (up to ~0.3mM O_2 and nM levels of $O_2^{\bullet -}$), $Mn^{II}P^{4+}$ however prefers reducing oxygen to superoxide (eq [3]) with relatively high rate constant, $k_{red}(O_2)$ (Figure 1B) (See further Discussion below under subtitle E2 vs. BuoE2). Eventually superoxide will dismute to H_2O_2 with or without SOD enzyme or its mimic (rate constant of $O_2^{\bullet -}$ self-dismutation, $k \sim 5 \times 10^5\ M^{-1}\ s^{-1}$). In parallel, deprotonated ascorbate radical, $A^{\bullet -}$, will undergo oxidation (i) with either oxygen to $O_2^{\bullet -}$ (eq [4]] (which would give rise to peroxide either through self- or enzyme-driven dismutation) (eq [4a]); or (ii) with $O_2^{\bullet -}$ (4b) and will ultimately produce peroxide [52] (Figure 8A). The rate constants for the reactions between ascorbate, O_2, and $O_2^{\bullet -}$ have been previously published [24]. The H_2O_2 is a major signaling species under nM levels, due to its long half-life and its ability to cross cell membranes [53]. The $k_{red}(O_2)$ for eq [3] (Figure 1B), was estimated primarily on thermodynamic grounds and is based on: (i) the metal-centered reduction potentials for $Mn^{III}P/Mn^{II}P$ redox couple, $E_{1/2}$ (Figure 1B); (ii) the Marcus equation where a change in $E_{1/2}$ of 120 mV induces 10-fold difference in a rate constant [54, 55]; and (iii) $k_{red}(O_2)$ for MnTM-4-PyP^{5+} [32, 46]. The estimation suffers from certain simplifications. Additional approach with initial rates for ascorbate (HA^-) oxidation with $Mn^{III}P$ was implemented and the data presented in Figure 1B. Both approaches were compared under subtitle: E2 *vs.* BuOE2.

The reactions described in equations [1] to [3] indicate that MnP/ascorbate system carries a therapeutic potential for cytotoxicity if certain conditions are met. The cellular balance between the oxidants and antioxidants would determine the outcome – cell survival or cell death. With excessive ascorbate levels added exogenously, under aerobic conditions, in the presence of an optimized catalyst for ascorbate oxidation, and with peroxide-removing enzymes down-regulated, the excessive production of peroxide could outbalance the cellular defense systems and could ultimately result in cell death. The extracellular action of MnP-based catalyst will depend upon (i) a fine ratio between the reducibility of MnP with ascorbate and its re-oxidation with oxygen (leading to H_2O_2 production); and (ii) the susceptibility of a catalyst to oxidative degradation. Both factors will depend upon the physical and chemical properties of a MnP catalyst.

The degradation of MnP (the loss of catalyst) occurs through its oxidation to $(O)_2Mn^{V}P$ species given by eq [5] [48, 49]. Presumably high-valent Mn, $(O)_2Mn^{V}P$, oxidizes the porphyrin ring which falls apart as noticed by the loss of color due to the loss of chromophoric structure of porphyrin ring [45]. *In vitro* and *in vivo*, the redox cycling of MnP between $(O)_2Mn^{V}P$ and $Mn^{III}P$ may occur at the expense of cellular reductants (shown for GSH in eq [6]) [51]. Therefore, in addition to the direct reaction of GSH with peroxide, GSH might have been consumed in this study in the reaction with Mn(V) or Mn(IV) species (Figure 3B) by eq [6]. Reduction of Mn(V) and Mn(IV) porphyrin species with other reductants is possible also [56]. The rate constants for the reduction of high-valent Mn(V) and Mn(IV) porphyrin oxo species with ascorbate, glutathione, *N*-acetyl cysteine, and uric acid to $Mn^{III}P$ are in the range of 4×10^4 for glutathione to $3 \times 10^6\ M^{-1}\ s^{-1}$ for ascorbate

[56]. The rate constant for the oxidation of cationic *ortho N*-alkylpyridylporphyrins with H_2O_2 producing $(O)_2Mn^{V}P$ species is estimated to be ~ 10^3 M^{-1} s^{-1} based on the reported reactivity of MnTM-2-PyP^{5+} [23, 47]. The reactive species of MnP towards H_2O_2 has been identified as monohydroxoaqua $Mn^{III}P$, eq[5] [51]:

$$(\mathrm{H_2O})\,(OH)\,Mn^{III}\mathrm{P}^{4+}+\mathrm{H_2O_2} \iff (\mathrm{O})_2 Mn^{\mathrm{V}}\mathrm{P}^{3+}+2 \quad \mathrm{H_2O}+\mathrm{H}^{+} \quad [5]$$

$$(\mathrm{O})_2 Mn^{\mathrm{V}}\mathrm{P}^{3+}+2 \quad GS^{\bullet}+4\mathrm{H}^{+} \iff (\mathrm{H_2O})_2 Mn^{III}\mathrm{P}^{5+}+GSSG \quad [6]$$

The MnP/reductant pro-oxidative system may be beneficial even in non-cancerous, yet diseased states. This was shown to be true in a recent study on a rat kidney/ischemia model where MnTnHex-2-PyP^{5+}, in a combination with a simple thiol, *N*-acetyl cysteine, induced a robust upregulation of endogenous antioxidants, including mitochondrial and extracellular superoxide dismutases among many others [57]. Since two SOD enzymes were upregulated, it is logical to assume that MnP had not acted as a SOD mimic in this instance. Redox cycling of MnP with *N*-acetyl cysteine produces mild pro-oxidative conditions, which in turn may have induced the adaptive responses observed in this model.

E2 *vs.* BuOE2. Based on thermodynamic parameters, *i.e.* Marcus equation, one would predict a faster rate of peroxide production with E2+asc rather than with BuOE2+asc system. Thus, upon the reduction with ascorbate, due to the more positive $E_{1/2}$, the Mn center of BuOE2 would be stabilized in the +2 oxidation state, and would thus be less prone than E2 to cycle back to $Mn^{III}P$ in order to produce peroxide; this is suggested with ~2.6-fold lower $k_{red}(O_2)$ of BuOE2 than E2 (Figure 1B), and with reappearance of $Mn^{III}P$ within 90 min for E2 and 125 min for BuOE2 post ascorbate addition (Figures 7A and B). The $k_{red}(O_2)$ (Figure 1B), which was estimated based on Marcus equation, suffers from certain limitations. The Marcus equation, which describes the electron transfer, was originally applied to predominantly outer-sphere reactions. It has been subsequently extended to inner-sphere- and heterogeneous reactions also. It assumes that the species reacting are weakly coupled and retain their individuality. The reaction of $Mn^{II}P$ with oxygen, relative to the reaction of $Mn^{II}P$ with superoxide (described by structure-activity relationships [22, 32], which obeys Marcus equation), likely involves the (transient) oxygen binding to Mn(II) and thus bears at least in part the inner-sphere character. Due to the involvement of binding, the magnitude of the reaction described by the $k_{red}(O_2)$ may be affected by trans-axial kinetic effect, which is ruled by the electron-deficiency of the Mn site. Also, the rate constants would, to some extent, be affected by the length of the *N*-pyridyl substituents which, if long, could impose steric hindrance towards the approach of oxygen (please see for further details references [22, 23, 50, 58]). Therefore, due to the interplay of different effects, the estimation of $k_{red}(O_2)$ based on Marcus equation is approximate (Figure 1).

The system explored herein is a complex as depicted in Figure 8. In addition to reduced and oxidized species of MnP and O_2, it involves differently protonated, reduced and oxidized ascorbate species, thus also complex protonation equilibria. We have therefore implemented the initial rate-approach to estimate the rates of HA^{-} oxidation by $Mn^{III}P$ which in case of

electron-efficient Mn porphyrins E2 and BuOE2 are limited by $Mn^{II}P$ re-oxidation. While it suffers from its own limitations, such an approach has been heavily utilized to solve the complex biological systems. It accounts for the event/s occurring during only short, initial periods of time, assuming those are fairly simple and result in a linear [HA^-] time response. The reaction of ascorbate, HA^-, with $Mn^{III}Ps$ likely involves ascorbate binding to Mn site. As with oxygen, differential binding of ascorbate to E2 or BuOE2 may be affected by: (i) differently shielded cationic charges on nitrogen by longer butoxyethyl chains than shorter ethyl chains; and (ii) differential electron-deficiency of E2 and BuOE2 Mn sites, described by $E_{1/2}$. Using initial rates these two compounds differ by ~30%; the calculated initial rates in M s^{-1} are given in Figure 1B. In addition to H_2O_2 arising from $Mn^{II}P$ oxidation with O_2 (due to the high levels of oxygen this reaction is preferred over the oxidation with $O_2^{\bullet-}$), there is a contribution in H_2O_2 formation from other reactions also: (i) the reaction of $Mn^{II}P$ with $O^{\bullet-}_2$; (ii) the reaction of HA^- with O_2; (iii) the reaction of $A^{\bullet-}$ with O_2; and (iv) the reaction of $A^{\bullet-}$ with $O_2^{\bullet-}$ (Figure 8) (Please see also [21, 24]). The formation of $Mn^{II}P$ *via* reduction of $Mn^{III}P$ with $A^{\bullet-}$ (eq [1b]) may contribute to $Mn^{III}P$/asc interactions as well. The initial rates approach does not account for the oxidative degradation of MnP. The porphyrin oxidative degradation, involving several reactions (complex in its own right, depicted in part with equation [5]), involves binding of peroxide to the metal site. It may be affected by the steric hindrance imposed by long butoxyethyl chains and perhaps by the presence of oxygen atoms in those chains [19, 23]. Our data do not allow us to assess the differences in MnP sensitivity to oxidative degradation. Based on Figure 7A, BuOE2 remains longer in the reaction mixture as compared to E2. However, this higher apparent stability of BuOE2 *vs* E2 might be a result of its slower production of H_2O_2. Further comparative exploration of a MnP/H_2O_2 system is needed.

The data obtained from biological assays are in reasonable agreement with kinetic data (Figure 1B). The differences in the loss of cell viability imposed by E2/acs and BuOE2/asc are given in Figures 2 and 3. The same loss in cell viability was achieved by 3-fold higher concentration of BuOE2 (Figure 2). In another experiment, the 30 μM E2/asc inflicts up to ~3-fold higher loss in cell viability than BuOE2 (Figure 3).

Neither kinetic approach describes accurately the interactions which gave rise to H_2O_2 in MnP/ascorbate system, but provide us with reasonable information on the differences between the BuOE2 and E2—To add an additional layer of the complexity to the MnP/ascorbate system, the transport into cells and the inner compartments (mitochondria, nucleus etc) would be greatly affected by up to ~5,000-fold difference in the lipophilicities of E2 and BuOE2 [27]. Therefore, the ultimate answer on the superiority of one MnP over the other will be provided by *in vivo* experiments.

Earlier reports on the cellular studies showed that extracellular peroxide, formed as a consequence of MnP/ascorbate interactions, is the cause of cell death [18, 59, 60]. Similar to our previous report [24], the ~5,000-fold difference in the lipophilicity of E2 and BuOE2 (Figure 1) is of no great importance in this cellular model of IBC. However, shape, planarity, lipophilicity, and in turn bioavailability will likely play a significant role in animal models and clinical settings. We have already shown that the lipophilic BuOE2 distributes to mitochondria (relative to cytosol) and crosses the blood brain barrier to a higher extent than

E2 [61]. A most dramatic example how lipophilicity can compensate for insufficient reactivity of Mn porphyrin has been the aerobic growth of SOD-deficient *E. coli* [62]. The *meta* isomeric MnTE-3-PyP^{5+} (E3), which has 10-fold lower $k_{cat}(O_2^{\bullet-})$, exhibits identical protection to aerobic growth of SOD-deficient *E. coli* as the *ortho* isomeric E2 due to its 10-fold higher lipophilicity [62].

Cellular pathways involved in cell death imposed by MnP/asc

Our data show that the rapid production of H_2O_2 led to decreased pro-survival ERK and NF-κB signaling (Fig. 8, *2*) and decreased mitochondrial integrity (Fig. 8, *3*). The cell death was dependent on ROS, specifically H_2O_2, as addition of exogenous catalase, effectively reversed cell death. Increased accumulation of ROS decreased *p*-NF-κB and *p*-ERK levels. This is of particular interest in IBC as high NF-κB activity is a feature of IBC pathogenesis [63, 64]. Another group has shown that, under conditions of increased H_2O_2 as a consequence of glucocorticoid treatment, and in the presence of glutathione, MnTE-2-PyP^{5+} would glutathionylate the p65 subunit of NF-κB and deplete GSH preventing its anti-apoptotic activity [17, 65]. Similar to our study, GSH levels were depleted with combination treatment.

Cell death parameters assayed in the E2+asc treated cells showed increased Annexin V positivity, decreased XIAP, and cleavage of the caspase substrate PARP, revealing apoptosis-mediated cytotoxicity in cells. Remarkably, addition of a potent pan-caspase inhibitor (Q-VD-OPh) did not reverse the cell death mediated by E2+asc. Correspondent with this inability to reverse cell death with a caspase inhibitor, we observed that in these treated cells, apoptosis inducing factor (AIF) was translocated to the nucleus (Fig. 8, *4*). AIF is a 67 kDa, mitochondria-localized flavoprotein that is known to activate caspase-independent cell death upon mitochondrial damage [66]. After cellular insult, AIF translocates to the nucleus and can cause cell death while also inducing classical apoptotic features such as phosphatidylserine exposure and chromatin condensation; this cell death mechanism has been shown to be PARP1-dependent in some systems, consistent with findings in Figure 5 [66-68]. This phenomenon of AIF induction after H_2O_2treatment has been reported in various cell types including B cells, myoblasts, and neurons, among others [68, 69]. Continuous influx of H_2O_2 was seen to induce caspase-independent cell death in Jurkat T cells [70]. Indeed, data in the current study show that the interaction between MnPs and ascorbate can continuously produce superoxide and hydrogen peroxide (until all ascorbate is consumed) (Fig. 8, *1*), which is most likely the cause for AIF-mediated, caspase-independent cell death in this pro-oxidant model. Conversely, in a model of cardiomyocytes, AIF nuclear translocation *via* doxorubicin-driven mitochondrial lipid peroxidation was attenuated by the administration of various MnPs alone [71]. The differential effects, pro-oxidative (with cancer cells) *vs.* anti-oxidative with cardiomyocytes (normal cell), are at least in part a consequence of differences in the cell types. These studies, along with our observations, support a caspase-independent mechanism of cell death induced by E2+ascorbate.

Therapeutic potential of MnP/asc system

Earlier work has shown the efficacy of pharmacological administration of ascorbate in treating cancer cells *in vitro* and *in vivo* [28, 59, 72] and paved the way to clinical trials. Ascorbate administration for 8 weeks increased both progression-free survival and overall survival in these clinical trials [29, 73].

Based on present understanding of anticancer therapy the most promising strategies would combine several approaches. We have already shown that MnTE-2-PyP^{5+} enhances radiation [19, 20, 61, 74] and glucocorticoid therapy [17, 65]. For the latter, the evidence was provided that it occurs via glutathionylation of NF-κB, catalyzed by MnP in the presence of H_2O_2 and GSH system. Future studies would clarify if the radiotherapy enhancement shares the same apoptotic pathways. In order to correctly predict which cancer cell type would be responsive to any of these strategies alone or combined, and at what ratio of MnP to ascorbate the system would be therapeutic, one would need to explore the ability of the cell to handle excess of peroxide. This would include the determination of the cellular redox environment, which would include the measurements of the levels and activities of cellular antioxidants.

MnTE-2-PyP^{5+} (E2) is available as GMP grade and a Phase I clinical trial in mice and monkeys has shown excellent safety/toxicity profile [75]. Such data provide the feasibility of the development of this compound in IBC therapy and pave the way to many other compounds that operate *via* similar mechanisms [23]. Our data show its high potential to play a role as anticancer drug and most so when administered with other compounds or anticancer modalities.

CONCLUDING REMARKS

The peroxide generating system MnP+ascorbate leads to cellular apoptosis in inflammatory breast cancer. Moreover, it overcame the high antioxidant-mediated apoptosis resistance in the rSUM149 aggressive breast cancer cellular model. Reduction of NF-κB and ERK pro-survival signaling as well as caspase-independent apoptosis was observed with MnP +ascorbate administration. The current study substantiates the therapeutic potential of a system where the metal-based catalyst favors redox cycling with ascorbate, producing peroxide, which along with its progeny, causes cell death. Further optimization of the system may be necessary to move forward with its development as anticancer treatment. Studies are needed to explore the redox status of each cancer type to be treated in order to correctly predict which one would be responsive to excessive levels of peroxide. This system may be combined with other therapeutic strategies that kill cancer cells *via* enhanced oxidative stress.

ACKNOWLEDGEMENTS

This work was supported by in part by funding from the American Cancer Society-RSG-08-290-01-CCE (G.R.Devi), Duke University Diversity Enhancement Fellowship (M.K. Evans), Duke Dean's Graduate Fellowship (M.K. Evans), and general research funds (I. Batinic-Haberle and A. Tovmasyan).

The authors would like to thank Amy Aldrich for technical support, Tao Wang (Dr. Kim Lyerly's laboratory) for flow cytometry support, Dr. Debra Silver for microscopy support, and also Dr. Mark Dewhirst, Dr. Scott Sauer, and Jennifer Allensworth for helpful discussion during preparation of the manuscript.

Abbreviations

AIF	apoptosis inducing factor
asc	ascorbate
BuOE2	MnTnBuOE-2-PyP^{5+} (BMX-001), Mn(III) *meso*-tetrakis(*N*-n-butoxyethyl-pyridinium-2yl) porphyrin
E2	MnTE-2-PyP^{5+} (AEOL10113, BMX-010), Mn(III) *meso*-tetrakis(*N*-ethyl-pyridinium-2yl) porphyrin
GSH	glutathione
IBC	inflammatory breast cancer
MnP	manganese porphyrin
ROS	reactive oxygen species
SOD	superoxide dismutase
XIAP	X-linked inhibitor of apoptosis

REFERENCES

1. Adler V, Yin Z, Tew KD, Ronai Z. Role of redox potential and reactive oxygen species in stress signaling. Oncogene. 1999; 18:6104–6111. [PubMed: 10557101]
2. Rada B, Leto TL. Oxidative innate immune defenses by Nox/Duox family NADPH oxidases. Contributions to microbiology. 2008; 15:164–187. [PubMed: 18511861]
3. Toure F, Fritz G, Li Q, Rai V, Daffu G, Zou YS, Rosario R, Ramasamy R, Alberts AS, Yan SF, Schmidt AM. Formin mDia1 mediates vascular remodeling via integration of oxidative and signal transduction pathways. Circ Res. 2012; 110:1279–1293. [PubMed: 22511750]
4. Ott M, Gogvadze V, Orrenius S, Zhivotovsky B. Mitochondria, oxidative stress and cell death. Apoptosis. 2007; 12:913–922. [PubMed: 17453160]
5. Agostinelli E, Seiler N. Non-irradiation-derived reactive oxygen species (ROS) and cancer: therapeutic implications. Amino Acids. 2006; 31:341–355. [PubMed: 16680401]
6. Fuchs-Tarlovsky V. Role of antioxidants in cancer therapy. Nutrition (Burbank, Los Angeles County, Calif.). 2013; 29:15–21.
7. Fang J, Nakamura H, Iyer AK. Tumor-targeted induction of oxystress for cancer therapy. Journal of drug targeting. 2007; 15:475–486. [PubMed: 17671894]
8. Fang J, Seki T, Maeda H. Therapeutic strategies by modulating oxygen stress in cancer and inflammation. Advanced drug delivery reviews. 2009; 61:290–302. [PubMed: 19249331]
9. Sies H. Strategies of antioxidant defense. European journal of biochemistry / FEBS. 1993; 215:213–219. [PubMed: 7688300]
10. Di Mascio P, Murphy ME, Sies H. Antioxidant defense systems: the role of carotenoids, tocopherols, and thiols. The American journal of clinical nutrition. 1991; 53:194S–200S. [PubMed: 1985387]
11. Gius D, Spitz DR. Redox signaling in cancer biology. Antioxid Redox Signal. 2006; 8:1249–1252. [PubMed: 16910772]
12. Trachootham D, Alexandre J, Huang P. Targeting cancer cells by ROS-mediated mechanisms: a radical therapeutic approach? Nature reviews. Drug discovery. 2009; 8:579–591.

13. Aird KM, Allensworth JL, Batinic-Haberle I, Lyerly HK, Dewhirst MW, Devi GR. ErbB1/2 tyrosine kinase inhibitor mediates oxidative stress-induced apoptosis in inflammatory breast cancer cells. Breast Cancer Res Treat. 2012; 132:109–119. [PubMed: 21559822]
14. Miriyala S, Spasojevic I, Tovmasyan A, Salvemini D, Vujaskovic Z, St Clair D, Batinic-Haberle I. Manganese superoxide dismutase, MnSOD and its mimics. Biochim Biophys Acta. 2012; 1822:794–814. [PubMed: 22198225]
15. Hempel N, Carrico PM, Melendez JA. Manganese superoxide dismutase (Sod2) and redox-control of signaling events that drive metastasis. Anti-cancer agents in medicinal chemistry. 2011; 11:191–201. [PubMed: 21434856]
16. Batinic-Haberle I, Rajic Z, Benov L. A combination of two antioxidants (an SOD mimic and ascorbate) produces a pro-oxidative effect forcing Escherichia coli to adapt via induction of oxyR regulon. Anti-cancer agents in medicinal chemistry. 2011; 11:329–340. [PubMed: 21355843]
17. Jaramillo MC, Briehl MM, Crapo JD, Batinic-Haberle I, Tome ME. Manganese porphyrin, MnTE-2-PyP5+, Acts as a pro-oxidant to potentiate glucocorticoid-induced apoptosis in lymphoma cells. Free Radic Biol Med. 2012; 52:1272–1284. [PubMed: 22330065]
18. Halliwell, B.; Gutteridge, JM. Free radicals in biology and medicine. 4th ed.. Oxford University Press; New York: 2007.
19. Batinic-Haberle I, Reboucas JS, Spasojevic I. Superoxide dismutase mimics: chemistry, pharmacology, and therapeutic potential. Antioxid Redox Signal. 2010; 13:877–918. [PubMed: 20095865]
20. Batinic-Haberle I, Rajic Z, Tovmasyan A, Reboucas JS, Ye X, Leong KW, Dewhirst MW, Vujaskovic Z, Benov L, Spasojevic I. Diverse functions of cationic Mn(III)N-substituted pyridylporphyrins, recognized as SOD mimics. Free Radic Biol Med. 2011; 51:1035–1053. [PubMed: 21616142]
21. Tovmasyan A, Sheng H, Weitner T, Arulpragasam A, Lu M, Warner DS, Vujaskovic Z, Spasojevic I, Batinic-Haberle I. Design, mechanism of action, bioavailability and therapeutic effects of mn porphyrin-based redox modulators. Medical principles and practice : international journal of the Kuwait University, Health Science Centre. 2013; 22:103–130.
22. Batinic-Haberle I, Spasojevic I, Stevens RD, Hambright P, Neta P, Okado-Matsumoto A, Fridovich I. New class of potent catalysts of O2.-dismutation. Mn(III) ortho-methoxyethylpyridyl- and di-ortho-methoxyethylimidazolylporphyrins. Dalton Trans. 2004:1696–1702. [PubMed: 15252564]
23. Batinic-Haberle I, Tovmasyan A, Roberts E, Vujaskovic Z, Leong KW, Spasojevic I. SOD therapeutics: Latest insights into their structure-activity relationships and impact upon the cellular redox-based pathways. Antioxid Redox Signal. 2013
24. Ye X, Fels D, Tovmasyan A, Aird KM, Dedeugd C, Allensworth JL, Kos I, Park W, Spasojevic I, Devi GR, Dewhirst MW, Leong KW, Batinic-Haberle I. Cytotoxic effects of Mn(III) N-alkylpyridylporphyrins in the presence of cellular reductant, ascorbate. Free Radic Res. 2011; 45:1289–1306. [PubMed: 21859376]
25. Rawal M, Schroeder SR, Wagner BA, Du J, Buettner GR, Cullen JJ. Potential of Manganoporphyrins to Enhance the Efficacy of Pharmacological Ascorbate in the Treatment of Pancreatic Cancer. Free Radical Biology and Medicine. 2012; 53(Supplement 2):S115.
26. Tian J, Peehl DM, Knox SJ. Metalloporphyrin synergizes with ascorbic acid to inhibit cancer cell growth through fenton chemistry. Cancer Biother Radiopharm. 2010; 25:439–448. [PubMed: 20735206]
27. Rajic Z, Benov L, Kos I, Tovmasyan A, Batinic-Haberle I. Cationic Mn Porphyrins Change Their Action from anti- to pro-oxidative in the Presence of Cellular Reductants: Relevance to understanding the beneficial therapeutic effects of SOD mimics in vivo. Free Radic Biol Med. 2010; 49:S194–S194.
28. Chen Q, Espey MG, Krishna MC, Mitchell JB, Corpe CP, Buettner GR, Shacter E, Levine M. Pharmacologic ascorbic acid concentrations selectively kill cancer cells: action as a pro-drug to deliver hydrogen peroxide to tissues. Proc Natl Acad Sci U S A. 2005; 102:13604–13609. [PubMed: 16157892]

29. Welsh JL, Wagner BA, van't Erve TJ, Zehr PS, Berg DJ, Halfdanarson TR, Yee NS, Bodeker KL, Du J, Roberts LJ 2nd, Drisko J, Levine M, Buettner GR, Cullen JJ. Pharmacological ascorbate with gemcitabine for the control of metastatic and node-positive pancreatic cancer (PACMAN): results from a phase I clinical trial. Cancer Chemother Pharmacol. 2013; 71:765–775. [PubMed: 23381814]
30. Aird KM, Ding X, Baras A, Wei J, Morse MA, Clay T, Lyerly HK, Devi GR. Trastuzumab signaling in ErbB2-overexpressing inflammatory breast cancer correlates with X-linked inhibitor of apoptosis protein expression. Mol Cancer Ther. 2008; 7:38–47. [PubMed: 18202008]
31. Aird KM, Ghanayem RB, Peplinski S, Lyerly HK, Devi GR. X-linked inhibitor of apoptosis protein inhibits apoptosis in inflammatory breast cancer cells with acquired resistance to an ErbB1/2 tyrosine kinase inhibitor. Mol Cancer Ther. 2010; 9:1432–1442. [PubMed: 20406946]
32. Batinic-Haberle I, Spasojevic I, Hambright P, Benov L, Crumbliss AL, Fridovich I. Relationship among Redox Potentials, Proton Dissociation Constants of Pyrrolic Nitrogens, and in Vivo and in Vitro Superoxide Dismutating Activities of Manganese(III) and Iron(III) Water-Soluble Porphyrins. Inorganic Chemistry. 1999; 38:4011–4022.
33. Rajic Z, Tovmasyan A, Spasojevic I, Sheng H, Lu M, Li AM, Gralla EB, Warner DS, Benov L, Batinic-Haberle I. A new SOD mimic, Mn(III) ortho N-butoxyethylpyridylporphyrin, combines superb potency and lipophilicity with low toxicity. Free Radic Biol Med. 2012; 52:1828–1834. [PubMed: 22336516]
34. Amantana A, London CA, Iversen PL, Devi GR. X-linked inhibitor of apoptosis protein inhibition induces apoptosis and enhances chemotherapy sensitivity in human prostate cancer cells. Mol Cancer Ther. 2004; 3:699–707. [PubMed: 15210856]
35. Abramoff MD, Magalhaes PJ, Ram SJ. Image Processing with ImageJ. Biophotonics International. 2004; 11:36–42.
36. Cali JJ, Niles A, Valley MP, O'Brien MA, Riss TL, Shultz J. Bioluminescent assays for ADMET. Expert opinion on drug metabolism & toxicology. 2008; 4:103–120. [PubMed: 18370862]
37. Spasojevic I, Colvin OM, Warshany KR, Batinic-Haberle I. New approach to the activation of anti-cancer pro-drugs by metalloporphyrin-based cytochrome P450 mimics in all-aqueous biologically relevant system. Journal of inorganic biochemistry. 2006; 100:1897–1902. [PubMed: 16965820]
38. Tovmasyan AG, Rajic Z, Spasojevic I, Reboucas JS, Chen X, Salvemini D, Sheng H, Warner DS, Benov L, Batinic-Haberle I. Methoxy-derivatization of alkyl chains increases the in vivo efficacy of cationic Mn porphyrins. Synthesis, characterization, SOD-like activity, and SOD-deficient E. coli study of meta Mn(III) N-methoxyalkylpyridylporphyrins. Dalton Trans. 2011; 40:4111–4121. [PubMed: 21384047]
39. Silvera D, Schneider RJ. Inflammatory breast cancer cells are constitutively adapted to hypoxia. Cell Cycle. 2009; 8:3091–3096. [PubMed: 19755858]
40. Allensworth JL, Aird KM, Aldrich AJ, Batinic-Haberle I, Devi GR. XIAP Inhibition and Generation of Reactive Oxygen Species Enhances TRAIL Sensitivity in Inflammatory Breast Cancer Cells. Mol Cancer Ther. 2012; 11:1518–1527. [PubMed: 22508521]
41. Mosmann T. Rapid colorimetric assay for cellular growth and survival: application to proliferation and cytotoxicity assays. J Immunol Methods. 1983; 65:55–63. [PubMed: 6606682]
42. Chae HJ, Kang JS, Byun JO, Han KS, Kim DU, Oh SM, Kim HM, Chae SW, Kim HR. Molecular mechanism of staurosporine-induced apoptosis in osteoblasts. Pharmacological research : the official journal of the Italian Pharmacological Society. 2000; 42:373–381. [PubMed: 10987998]
43. Son YO, Jang YS, Heo JS, Chung WT, Choi KC, Lee JC. Apoptosis-inducing factor plays a critical role in caspase-independent, pyknotic cell death in hydrogen peroxide-exposed cells. Apoptosis. 2009; 14:796–808. [PubMed: 19418225]
44. Gallego MA, Joseph B, Hemstrom TH, Tamiji S, Mortier L, Kroemer G, Formstecher P, Zhivotovsky B, Marchetti P. Apoptosis-inducing factor determines the chemoresistance of non-small-cell lung carcinomas. Oncogene. 2004; 23:6282–6291. [PubMed: 15286713]
45. Spasojević I, Batinić-Haberle I. Manganese(III) complexes with porphyrins and related compounds as catalytic scavengers of superoxide. Inorganica Chimica Acta. 2001; 317:230–242.

46. Spasojevic I, Batinic-Haberle I, Fridovich I. Nitrosylation of manganese(II) tetrakis(N-ethylpyridinium-2-yl)porphyrin: a simple and sensitive spectrophotometric assay for nitric oxide. Nitric Oxide. 2000; 4:526–533. [PubMed: 11020341]

47. Jin N, Lahaye DE, Groves JT. A “push-pull” mechanism for heterolytic o-o bond cleavage in hydroperoxo manganese porphyrins. Inorg Chem. 2010; 49:11516–11524. [PubMed: 21080695]

48. Ferrer-Sueta G, Quijano C, Alvarez B, Radi R. Reactions of manganese porphyrins and manganese-superoxide dismutase with peroxynitrite. Methods Enzymol. 2002; 349:23–37. [PubMed: 11912912]

49. Groves JT, Lee J, Marla SS. Detection and Characterization of an Oxomanganese(V) Porphyrin Complex by Rapid-Mixing Stopped-Flow Spectrophotometry. Journal of the American Chemical Society. 1997; 119:6269–6273.

50. Tovmasyan A, Weitner T, Sheng H, Lu M, Rajic Z, Warner DS, Spasojevic I, Reboucas JS, Benov L, Batinic-Haberle I. Differential Coordination Demands in Fe versus Mn Water-Soluble Cationic Metalloporphyrins Translate into Remarkably Different Aqueous Redox Chemistry and Biology. Inorg Chem. 2013; 52:5677–5691. [PubMed: 23646875]

51. Batinic-Haberle I, Spasojevic I, Tse HM, Tovmasyan A, Rajic Z, St Clair DK, Vujaskovic Z, Dewhirst MW, Piganelli JD. Design of Mn porphyrins for treating oxidative stress injuries and their redox-based regulation of cellular transcriptional activities. Amino Acids. 2012; 42:95–113. [PubMed: 20473774]

52. Scarpa M, Stevanato R, Viglino P, Rigo A. Superoxide ion as active intermediate in the autoxidation of ascorbate by molecular oxygen. Effect of superoxide dismutase. J Biol Chem. 1983; 258:6695–6697. [PubMed: 6304051]

53. Forman HJ, Maiorino M, Ursini F. Signaling functions of reactive oxygen species. Biochemistry. 2010; 49:835–842. [PubMed: 20050630]

54. Marcus RA. Chemical + Electrochemical Electron-Transfer Theory. Annu Rev Phys Chem. 1964; 15:155–&.

55. Marcus RA. On Theory of Electron-Transfer Reactions .6. Unified Treatment for Homogeneous and Electrode Reactions. J Chem Phys. 1965; 43:679–&.

56. Ferrer-Sueta G, Batinic-Haberle I, Spasojevic I, Fridovich I, Radi R. Catalytic scavenging of peroxynitrite by isomeric Mn(III) N-methylpyridylporphyrins in the presence of reductants. Chem Res Toxicol. 1999; 12:442–449. [PubMed: 10328755]

57. Cohen J, Dorai T, Ding C, Batinic-Haberle I, Grasso M. The administration of renoprotective agents extends warm ischemia in a rat model. Journal of endourology / Endourological Society. 2013; 27:343–348. [PubMed: 23102208]

58. Spasojevic I, Batinic-Haberle I, Reboucas JS, Idemori YM, Fridovich I. Electrostatic contribution in the catalysis of O2*- dismutation by superoxide dismutase mimics. MnIIITE-2-PyP5+ versus MnIIIBr8T-2-PyP+. J Biol Chem. 2003; 278:6831–6837. [PubMed: 12475974]

59. Chen Q, Espey MG, Sun AY, Pooput C, Kirk KL, Krishna MC, Khosh DB, Drisko J, Levine M. Pharmacologic doses of ascorbate act as a prooxidant and decrease growth of aggressive tumor xenografts in mice. Proc Natl Acad Sci U S A. 2008; 105:11105–11109. [PubMed: 18678913]

60. Ranzato E, Biffo S, Burlando B. Selective ascorbate toxicity in malignant mesothelioma: a redox Trojan mechanism. Am J Respir Cell Mol Biol. 2011; 44:108–117. [PubMed: 20203294]

61. Batinic-Haberle I, Tovmasyan A, Roberts E, Vujaskovic Z, Leong KW, Spasojevic I. SOD therapeutics: Latest insights into the structure-activity relationships and cellular redox-based pathways - lessons from cancer and radiation studeis. Antioxid Redox Signal Under Revision. 2013

62. Kos I, Benov L, Spasojevic I, Reboucas JS, Batinic-Haberle I. High lipophilicity of meta Mn(III) N-alkylpyridylporphyrin-based superoxide dismutase mimics compensates for their lower antioxidant potency and makes them as effective as ortho analogues in protecting superoxide dismutase-deficient Escherichia coli. J Med Chem. 2009; 52:7868–7872. [PubMed: 19954250]

63. Van Laere SJ, Van der Auwera I, Van den Eynden GG, Elst HJ, Weyler J, Harris AL, van Dam P, Van Marck EA, Vermeulen PB, Dirix LY. Nuclear factor-kappaB signature of inflammatory breast cancer by cDNA microarray validated by quantitative real-time reverse transcription-PCR,

immunohistochemistry, and nuclear factor-kappaB DNA-binding. Clin Cancer Res. 2006; 12:3249–3256. [PubMed: 16740744]

64. Van Laere SJ, Van der Auwera I, Van den Eynden GG, van Dam P, Van Marck EA, Vermeulen PB, Dirix LY. NF-kappaB activation in inflammatory breast cancer is associated with oestrogen receptor downregulation, secondary to EGFR and/or ErbB2 overexpression and MAPK hyperactivation. Br J Cancer. 2007; 97:659–669. [PubMed: 17700572]
65. Jaramillo MC, Briehl MM, Tome ME. Manganese Porphyrin Glutathionylates the p65 Subunit of NF-κB to Potentiate Glucocorticoid-induced Apoptosis in Lymphoma. Free Radic Biol Med. 2010; 49:S63–S63.
66. Lorenzo HK, Susin SA, Penninger J, Kroemer G. Apoptosis inducing factor (AIF): a phylogenetically old, caspase-independent effector of cell death. Cell Death Differ. 1999; 6:516–524. [PubMed: 10381654]
67. Loeffler M, Daugas E, Susin SA, Zamzami N, Metivier D, Nieminen AL, Brothers G, Penninger JM, Kroemer G. Dominant cell death induction by extramitochondrially targeted apoptosis-inducing factor. Faseb J. 2001; 15:758–767. [PubMed: 11259394]
68. Yu SW, Wang H, Poitras MF, Coombs C, Bowers WJ, Federoff HJ, Poirier GG, Dawson TM, Dawson VL. Mediation of poly(ADP-ribose) polymerase-1-dependent cell death by apoptosis-inducing factor. Science. 2002; 297:259–263. [PubMed: 12114629]
69. Qiu XZ, Yu L, Lai GH, Wang LY, Chen B, Ouyang J. Mitochondrial AIF protein involved in skeletal muscle regeneration. Cell Biochem Funct. 2008; 26:598–602. [PubMed: 18508388]
70. Barbouti A, Doulias PT, Nousis L, Tenopoulou M, Galaris D. DNA damage and apoptosis in hydrogen peroxide-exposed Jurkat cells: bolus addition versus continuous generation of H(2)O(2). Free Radic Biol Med. 2002; 33:691–702. [PubMed: 12208356]
71. Miriyala S, Thipakkom C, Xu Y, Prachayasittikul V, Noel T, St Clair D. 4-hydroxy-2-nonenal Mediates AIFm2 Release from Mitochondria: An Insight into the Mechanism of Oxidative Stress Mediated Retrograde Signaling. Free Radic Biol Med. 2010; 49:S170–S170.
72. Chen Q, Espey MG, Sun AY, Lee JH, Krishna MC, Shacter E, Choyke PL, Pooput C, Kirk KL, Buettner GR, Levine M. Ascorbate in pharmacologic concentrations selectively generates ascorbate radical and hydrogen peroxide in extracellular fluid in vivo. Proc Natl Acad Sci U S A. 2007; 104:8749–8754. [PubMed: 17502596]
73. Monti DA, Mitchell E, Bazzan AJ, Littman S, Zabrecky G, Yeo CJ, Pillai MV, Newberg AB, Deshmukh S, Levine M. Phase I evaluation of intravenous ascorbic acid in combination with gemcitabine and erlotinib in patients with metastatic pancreatic cancer. PLoS One. 2012; 7:e29794. [PubMed: 22272248]
74. Moeller BJ, Batinic-Haberle I, Spasojevic I, Rabbani ZN, Anscher MS, Vujaskovic Z, Dewhirst MW. A manganese porphyrin superoxide dismutase mimetic enhances tumor radioresponsiveness. Int J Radiat Oncol Biol Phys. 2005; 63:545–552. [PubMed: 16168847]
75. Gad SC, Sullivan DW Jr. Crapo JD, Spainhour CB. A Nonclinical Safety Assessment of MnTE-2-PyP, a Manganese Porphyrin. International journal of toxicology. 2013
76. Williams NH, Yandell JK. Outer-Sphere Electron-Transfer Reactions of Ascorbate Anions. Aust J Chem. 1982; 35:1133–1144.

A

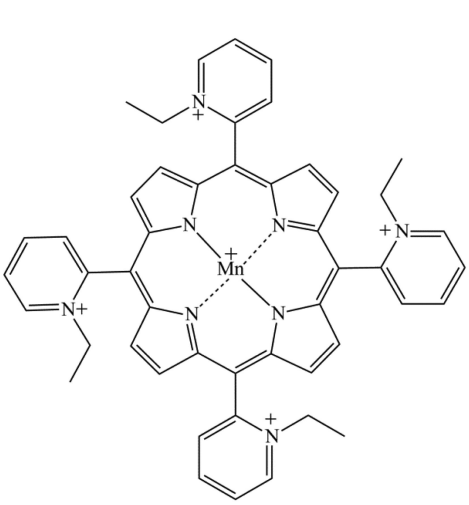

MnTE-2-PyP^{5+} (E2)

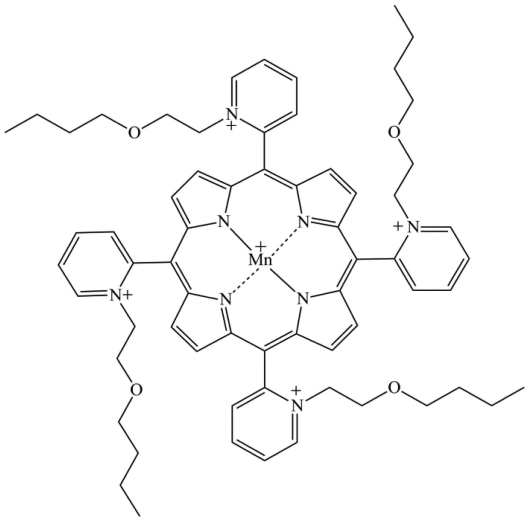

MnTnBuOE-2-PyP^{5+} (BuOE2)

B

Parameters	MnTE-2-PyP^{5+}	MnTnBuOE-2-PyP^{5+}
$k_{cat}(O_2^{\bullet-})$, M^{-1} s^{-1}	5.75×10^7	6.76×10^7
$k_{red}(O_2)$, M^{-1} s^{-1}	8×10^4	3×10^4
v_o $[(HA^-)_{ox}]$, M s^{-1}	1.7×10^{-7}	1.2×10^{-7}
$E_{1/2}$, mV *vs.* NHE	+228	+277
log P_{ow}	-7.79	-4.10

Figure 1. Structure, physicochemical characteristics, and redox properties of two Mn porphyrins used in this study

A) Chemical structures for the two manganese porphyrins MnTE-2-PyP^{5+} (E2) and MnTnBuOE-2-PyP^{5+} (BuOE2) used in this study**. B)** Table contains the catalytic rate constant for $O_2^{\bullet-}$ dismutation, $k_{cat}(O_2^{\bullet-})$, which describes their SOD-like activities; the rate constant for one-electron reduction of molecular oxygen, O_2, to superoxide, $O_2^{\bullet-}$, $k_{red}(O_2)$; the initial rate of ascorbate oxidation, v_o $[(HA^-)_{ox}]$; the metal-centered reduction potential for $Mn^{III}P/Mn^{II}P$ redox couple, $E_{1/2}$ in mV *vs.* NHE; and the partition coefficient for n-octanol and water (log P_{ow},) as a measure of lipophilicity. The values presented were

compiled from [24, 33]. Two kinetic approaches were used to evaluate the efficacy of MnPs as catalysts in the ascorbate-oxidation driven H_2O_2 production: Marcus equation and initial rates. [a]The $k_{red}(O_2)$ was estimated based on Marcus equation as previously reported [46]. [b]The initial rates of ascorbate oxidation by MnPs, were determined spectrophotometrically following the decrease in the ascorbate absorption at 265 nm over 5 minutes.

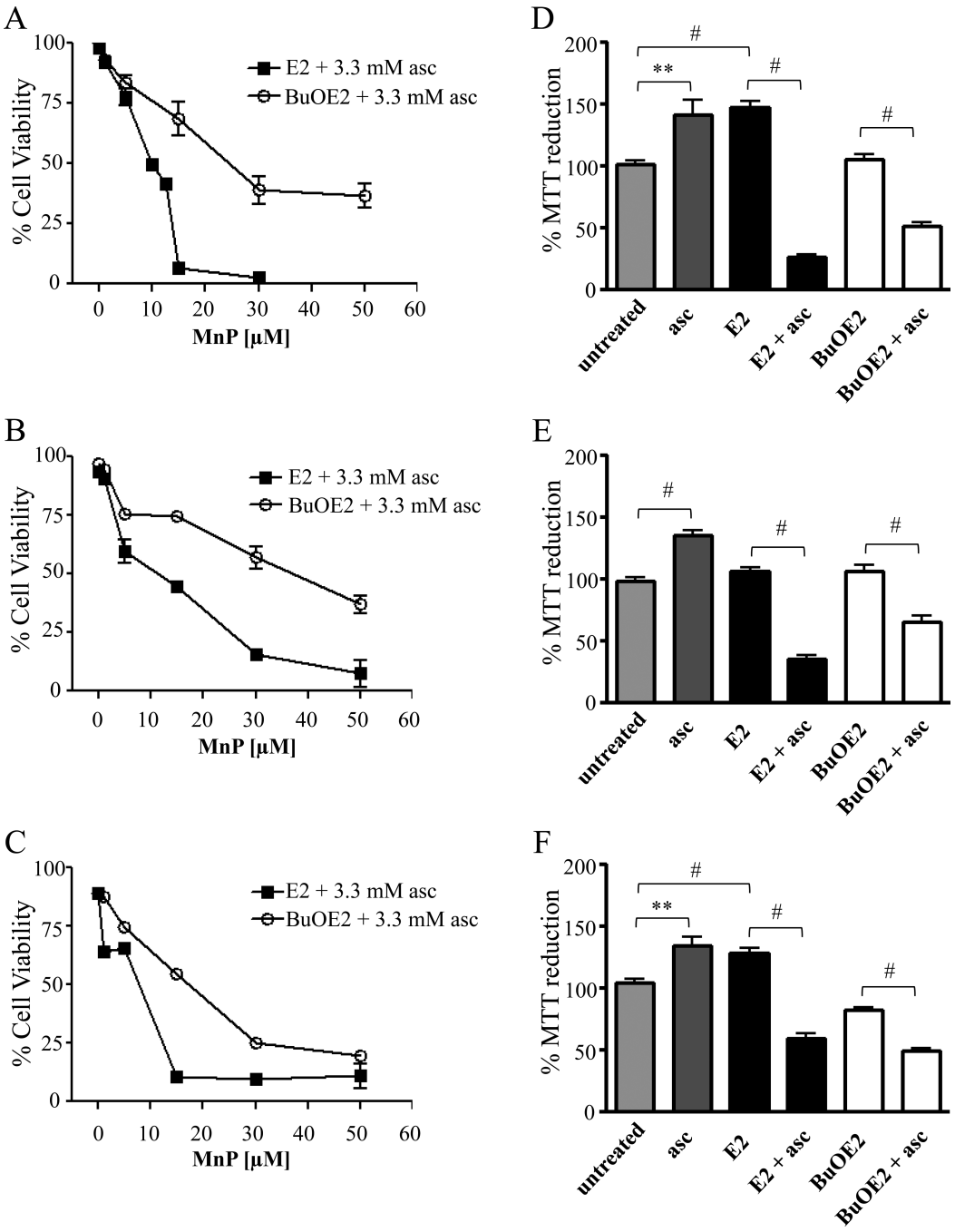

Figure 2. MnP+asc treatment enhances cell death in IBC cells

A) SUM149, B) rSUM149, and C) SUM190 viability as determined by trypan blue exclusion of cells treated with E2 or BuOE2 (0-50 μM) in the presence of ascorbate (3.3 mM) measured after 24 hours. Data represent mean±SEM viable cells taken as a percentage of total cells (n=2-3). MTT reduction of D) SUM149, E) rSUM149, and F) SUM190 cells treated with E2 or BuOE2 (50 μM) or ascorbate (3.3 mM), alone and in combination. Bars represent mean±SEM (n=8-16, **p<0.005, #p<0.001).

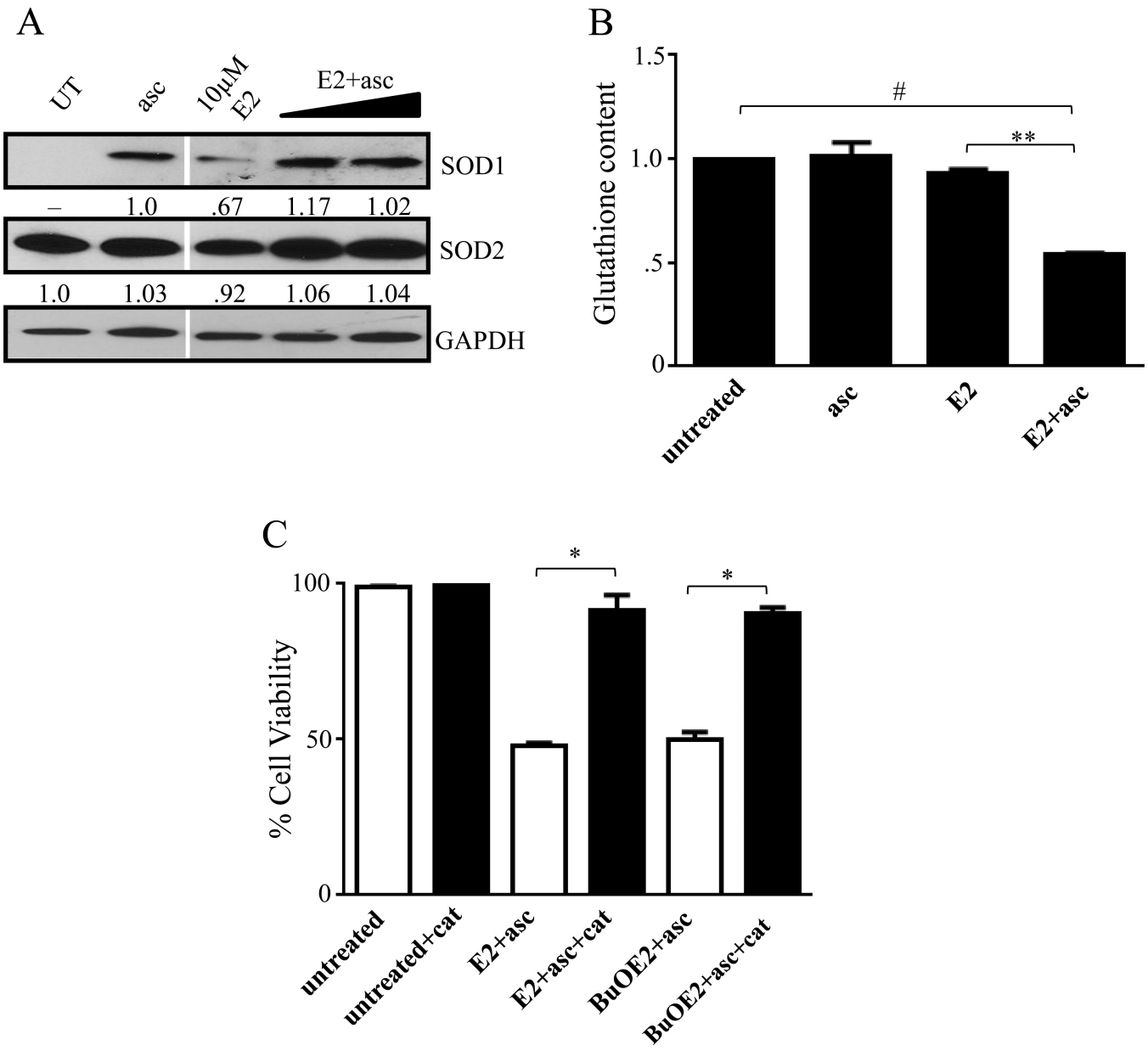

Figure 3. MnP+asc acts as a pro-oxidant in IBC cells

A) Western immunoblot analysis of SOD1 and SOD2. E2 doses in combination with 3.3 mM ascorbate: 1 μM and 10 μM. GAPDH was used as control. Numbers represent densitometric analysis compared to untreated, except 3A (top) where compared to ascorbate. B) GSH content of cells treated with ascorbate, E2 alone (10 μM), or the combination for 4 hours. Bars represent mean±SEM (n=2-3, *p<0.05, **p<0.005). C) Viability of SUM149 cells treated with the combination of E2+asc (10 μM) or BuOE2+asc (30 μM) in the presence or absence of 1500 U/mL catalase, after 24 hours. Bars represent mean±SEM (n=2-3, *p<0.05, **p<0.005).

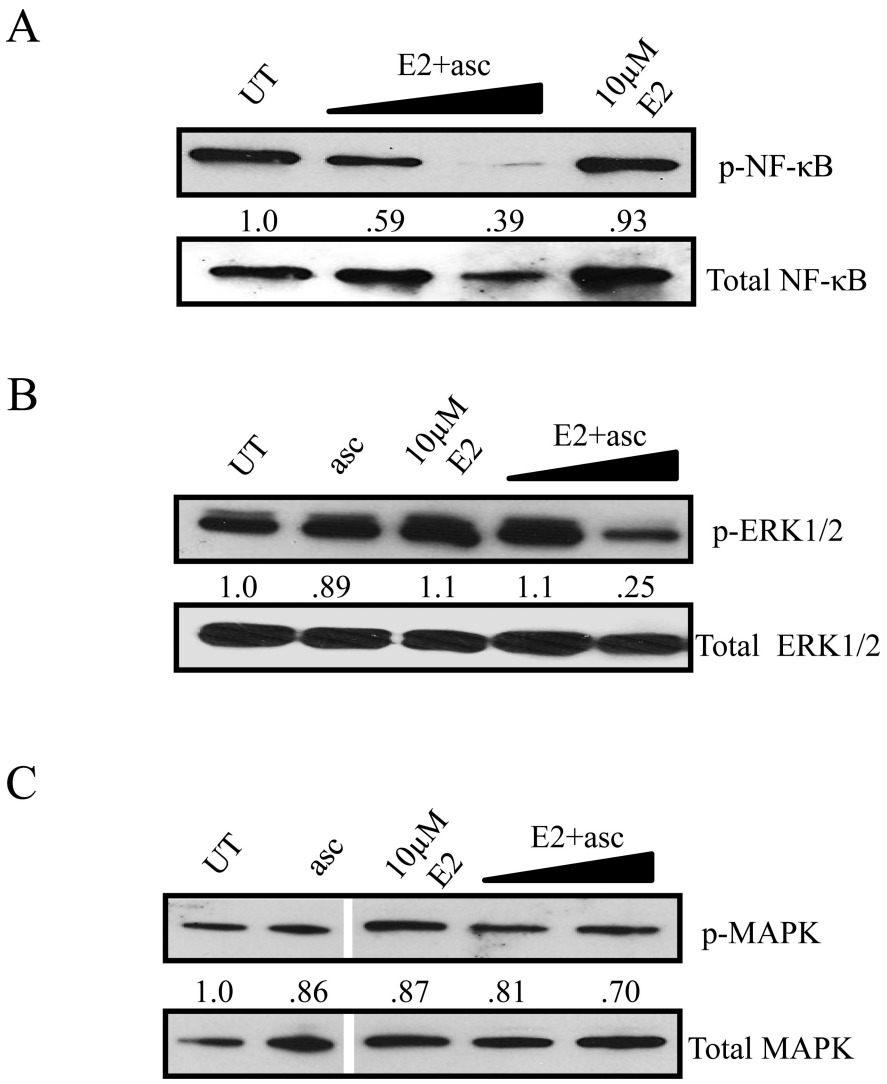

Figure 4. H_2O_2 production is essential for cytotoxicity and reduces pro-survival signaling by antagonizing redox sensors

A) Phosphorylated ERK1/2, B) phosphorylated NF-κB, and C) phosphorylated MAPK in SUM149 cells treated with ascorbate or E2, alone and in combination. E2 doses in combination with 3.3 mM ascorbate: 1 μM and 10 μM. Total ERK1/2, total NF-κB, or total MAPK, and GAPDH (not shown) were used as loading controls. Numbers represent densitometric analysis compared to untreated.

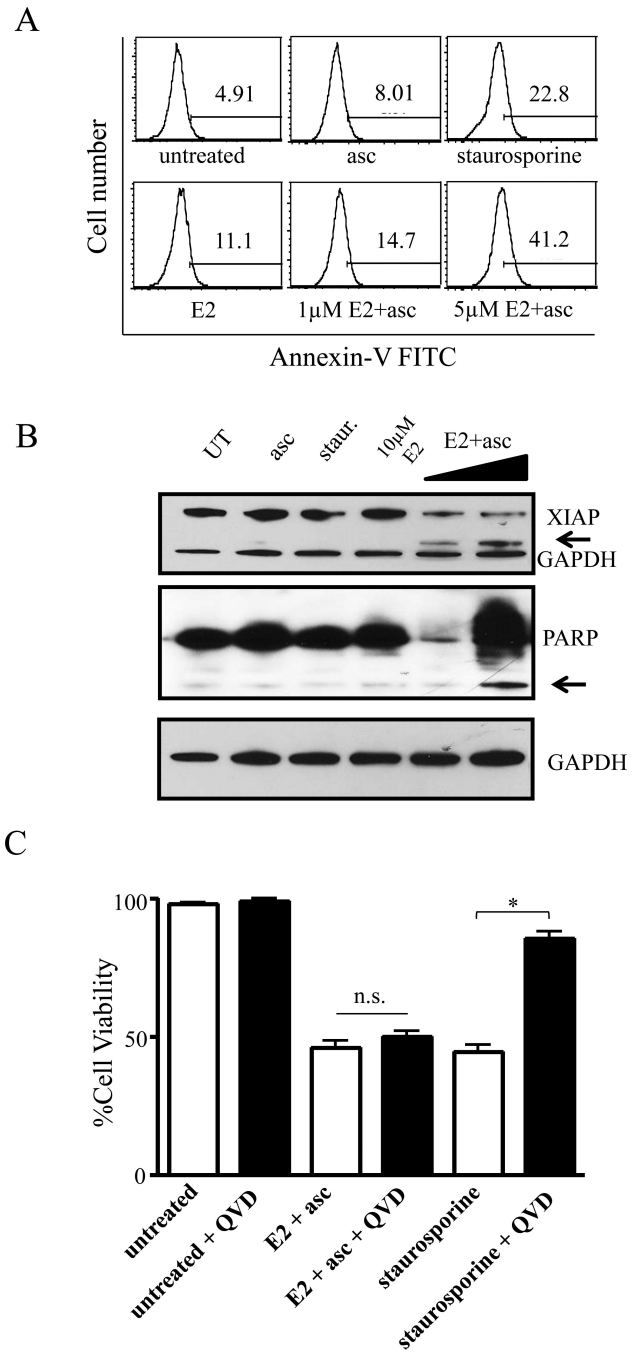

Figure 5. Cell death caused by MnP+asc shows classical markers of apoptosis, but is caspase-independent

A) SUM149 cells were treated with sublethal doses (corresponding to EC_{10} and EC_{25}, respectively) of E2 ± ascorbate or ascorbate alone for 4h and stained with Annexin-FITC. Histograms shown are representative of 2-3 independent experiments. Staurosporine was used as a control. B) Western immunoblot analysis of X-linked inhibitor of apoptosis (XIAP, top panel) and poly-ADP ribose polymerase (PARP, middle panel) in SUM149 cells treated with ascorbate or E2, alone and in combination. E2 doses in combination with 3.3 mM ascorbate: 1 μM and 10 μM. GAPDH was used as loading control. *Arrows denote*

cleavage products. C) Viability as determined by trypan blue exclusion assay of SUM149 cells treated with 10 μM E2+ascorbate or staurosporine for 24 hours, alone (white bars) or after 30 minute pre-treatment with 20 μM QVD-OPh (black bars), a pan-caspase inhibitor. Data represent mean±SEM viable cells taken as a percentage of total cells (n=2-3, *p<0.05).

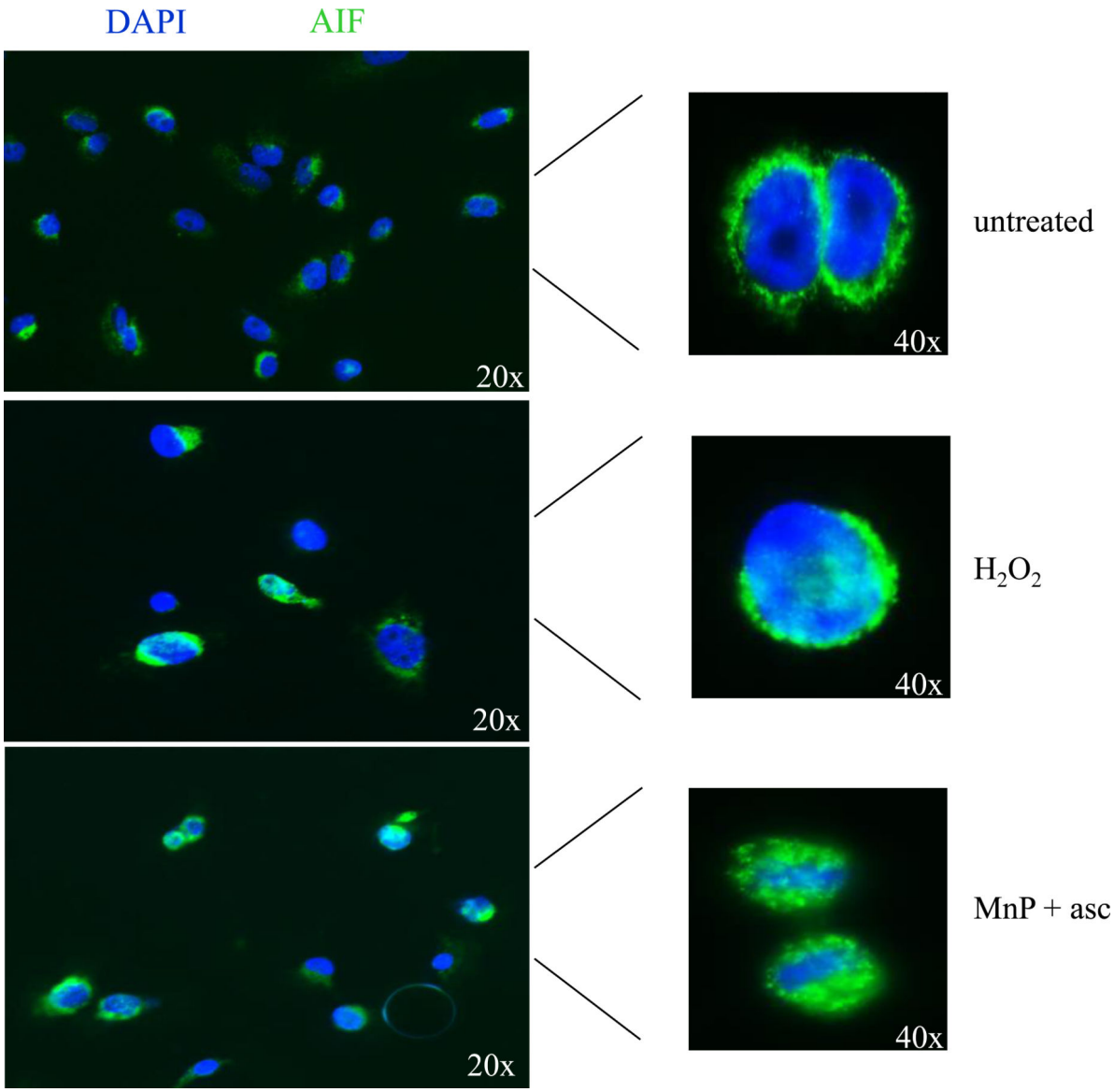

Figure 6. Translocation of apoptosis-inducing factor to the nucleus is observed after combination treatment with MnP+asc

Immunofluorescence images of cells stained with a monoclonal anti-AIF antibody taken with an inverted fluorescence microscope. Cells were left either untreated (*top*), treated with 500 μM H_2O_2 (*middle*), or ~EC_{50} dose of E2+asc (10 μM) or BuOE2+asc (30 μM) (*bottom*, E2+asc shown) for four hours and counterstained with DAPI before analysis. A representative result (both 20x and 40x) from two independent experiments is shown.

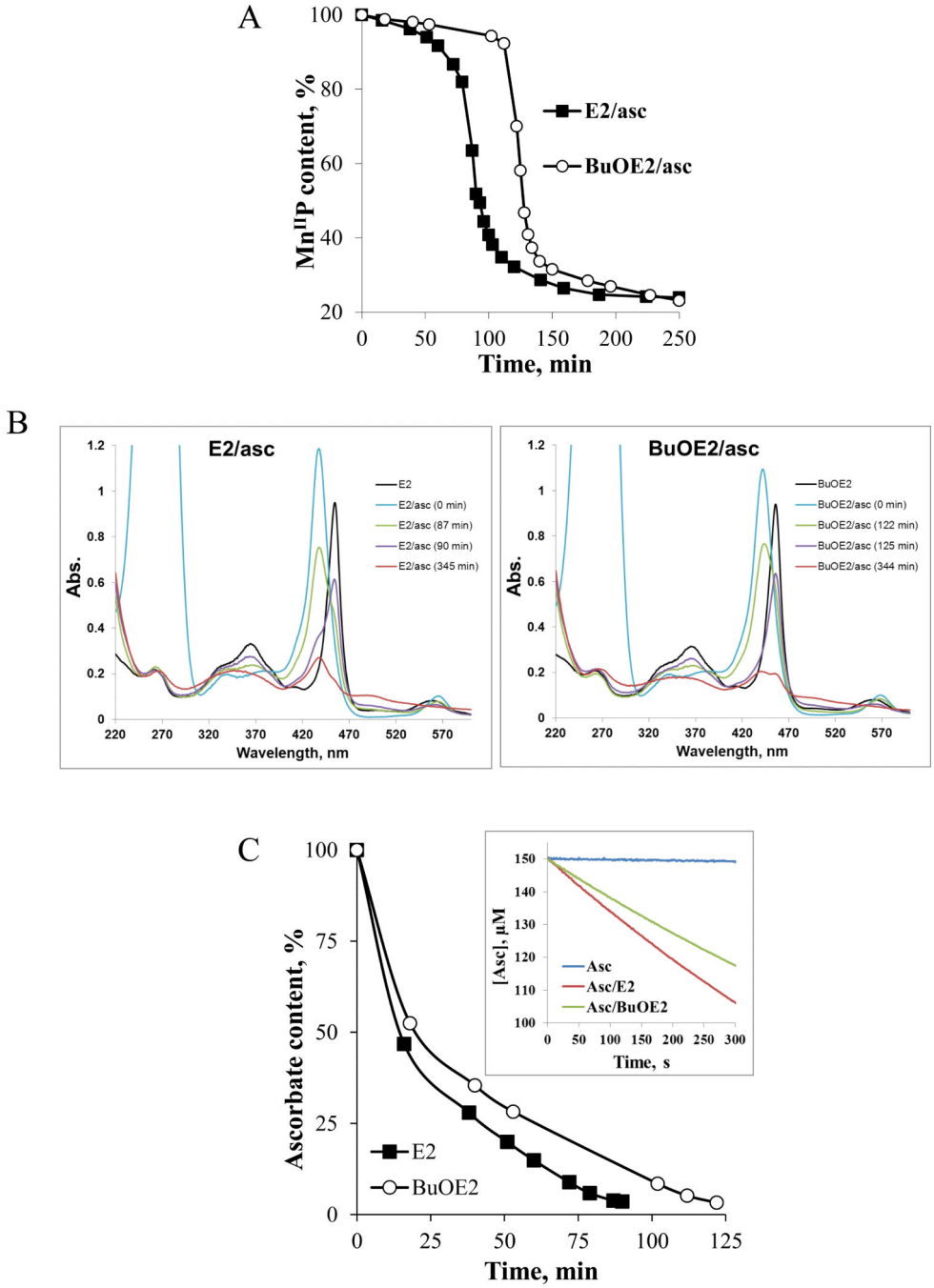

Figure 7. H_2O_2-driven degradation of Mn porphyrins in the presence of ascorbate, and oxidation/consumption of ascorbate

A) Ascorbate (0.42 mM)-driven reduction of $Mn^{III}P$ (6 μM) and its subsequent H_2O_2-driven oxidative degradation , as registered spectrophotometrically at the Soret band of the reduced $Mn^{II}P$ (437.5 nm for E2 and 441.5 nm for BuOE2) ; as Mn oxo species appear over time, our data do not allow for the assessment of the total MnP content. As long as ascorbate was present in solution it kept reduced $Mn^{II}P$ in solution (indicated as flat line); once ascorbate is consumed and peroxide accumulated, $Mn^{II}P$ gets reoxidized to $Mn^{III}P$ which subsequently reacts with H_2O_2. The oxidation of MnP with H_2O_2 leads to its degradation and is indicated

with a large drop in MnP absorption (see below); **B) and C)** Time dependent spectral change of MnPs in the presence of ascorbate. The first spectrum was recorded in the absence of ascorbate (HA^-), described as E2 or BuOE2, and relates to $Mn^{III}P$. Upon addition of ascorbate, the $Mn^{III}P$ got reduced to $Mn^{II}P$ (E2/asc, 0 min and BuOE2/asc, 0 min) which stays present in solution as long as there is ascorbate available. Once the ascorbate is consumed (disappearance of band at 265 nm), under aerobic conditions, the MnP ceased to be maintained in a reduced form. Consequently, the disappearance of the reduced $Mn^{II}P$ was observed, which was accompanied with the reappearance of $Mn^{III}P$ (~90 min for E2 and 125 min for BuOE2). The $Mn^{III}P$ subsequently got oxidized with H_2O_2 to a highly oxidizing Mn(V) oxo species, $(O)_2Mn^{V}P$ (eq [5]), which in turn oxidizes the porphyrin ring thus leading to its degradation. The $(O)_2Mn^{V}P$ readily decays to $O=Mn^{IV}P$ [48, 49]. The Soret bands of differently oxidized/reduced E2 species, that are present in solution at time-dependent ratios, are: $Mn^{II}P$ at 438 nm, $\varepsilon = 1.81 \times 10^5\ M^{-1}\ s^{-1}$, $Mn^{III}P$ at 454 nm, $\varepsilon = 1.29 \times 10^5\ M^{-1}\ s^{-1}$, $O=Mn^{IV}P$ at 425 nm, $\varepsilon = 9.0 \times 10^4\ M^{-1}\ s^{-1}$, and $(O)_2Mn^{V}P$ (pH 14) at 433 nm, $\varepsilon = 1.38 \times 10^5\ M^{-1}\ cm^{-1}$ [49]. **C)** Time-dependent oxidation/consumption of ascorbate, based on the spectrophotometric measurements of ascorbate at 265 nm, is accompanied by peroxide accumulation in the system. **Inset of Figure 7C:** Initial rates of ascorbate oxidation catalyzed by two Mn porphyrins differ by ~30%. The conditions are: 5 μM MnP, 150 μM ascorbate in 50 mM Tris buffer (pH 7.8). Initial rates are: for noncatalyzed HA^- oxidation, $v_o(HA^-)_{ox} = 3.0 \times 10^{-9}\ M\ s^{-1}$; for E2-catalyzed HA^- oxidation, $v_o(HA^-)_{ox} = 1.7 \times 10^{-7}\ M\ s^{-1}$; and for BuOE2-catalyzed HA^- oxidation $v_o(HA^-)_{ox} = 1.2 \times 10^{-7}\ M\ s^{-1}$ (Figure 1B). All experiments were performed in a cell-free tris-buffered system (pH 7.8).

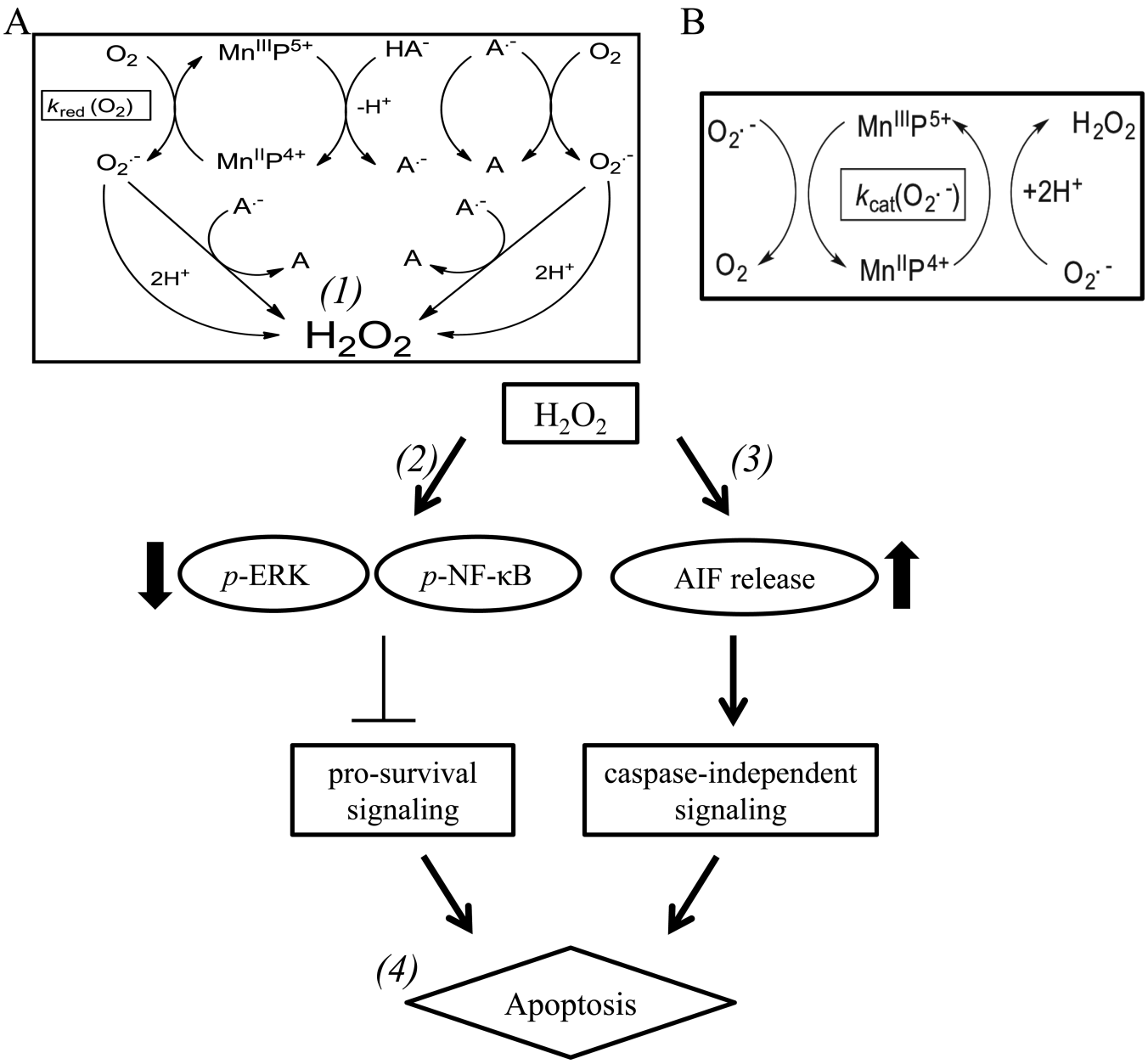

Figure 8. Interaction of MnP with ascorbate which leads to peroxide production

A) $Mn^{III}P$ reacts with ascorbate (HA^-), to form ascorbyl radical ($A^{\bullet-}$) and $Mn^{II}P$. $Mn^{II}P$ undergoes re-oxidation with oxygen (O_2, rate constant ~10^4-10^5 M^{-1} s^{-1}) to form superoxide ($O_2^{\bullet-}$), which readily dismutes with and without SOD enzyme into H_2O_2 *(1)*. In aqueous solution the oxygen concentration is orders of magnitude higher than that of superoxide, making this reaction more preferred than reaction of $Mn^{II}P$ with $O^{\cdot-}_2$. Superoxide can also react with ascorbyl radical to form H_2O_2 at a rate constant of >10^8 M^{-1} s^{-1} *(1)*. Ascorbyl radical, $A^{\bullet-}$ could be oxidized further with oxygen to form dehydroascorbate, A, giving rise to superoxide and eventually peroxide. Ascorbyl radical, $A^{\cdot-}$ could also be oxidized to A with $Mn^{III}P$. $A^{\cdot-}$ will self-dismute at a rate constant of ~10^5 M^{-1} s^{-1} [76]. **B)** $Mn^{II}P$ will also undergo a reaction with superoxide (rate constant ~5 × 10^7

M^{-1} s^{-1}) to form peroxide. Subsequently, the increased peroxide production leads to decreased phosphorylated p-ERK and p-NF-κB levels in cells (*2*). Increased ROS levels also can lead to permeabilization of the outer membrane of the mitochondria and to the release of apoptosis-inducing factor from the mitochondria (*3*). Upon release, AIF translocates to the nucleus, and can mediate caspase-independent cell death (*4*).

Table 1

Calculated, approximate EC_{50} (in μM) of each MnP+ascorbate combination in the SUM149 isogenic lines.

	SUM149	rSUM149	SUM190
MnTE-2-Pyp^{5+} (E2)	11.3±1.1	12.5±1.5	10.2±1.8
MnTnBuOE-2-PyP^{5+} (BuOE2)	30.0±1.3	39.9±3.2	17.1±1.5